Batteries & Supercaps

Review
doi.org/10.1002/batt.202400522

Chemistry Europe
European Chemical Societies Publishing

www.batteries-supercaps.org

Customized Nano-Confinement Effects of Metal-Organic Frameworks for High-Performance Lithium-Sulfur Batteries

Jingqia Weng,[a] Haibin Lu,[a] Qinghan Zeng,[a] Yingbo Xiao,[a] Junhua Yang,[a] Jionghui Rong,[a] Qi Zhang,*[a, b] and Shaoming Huang*[a, c]

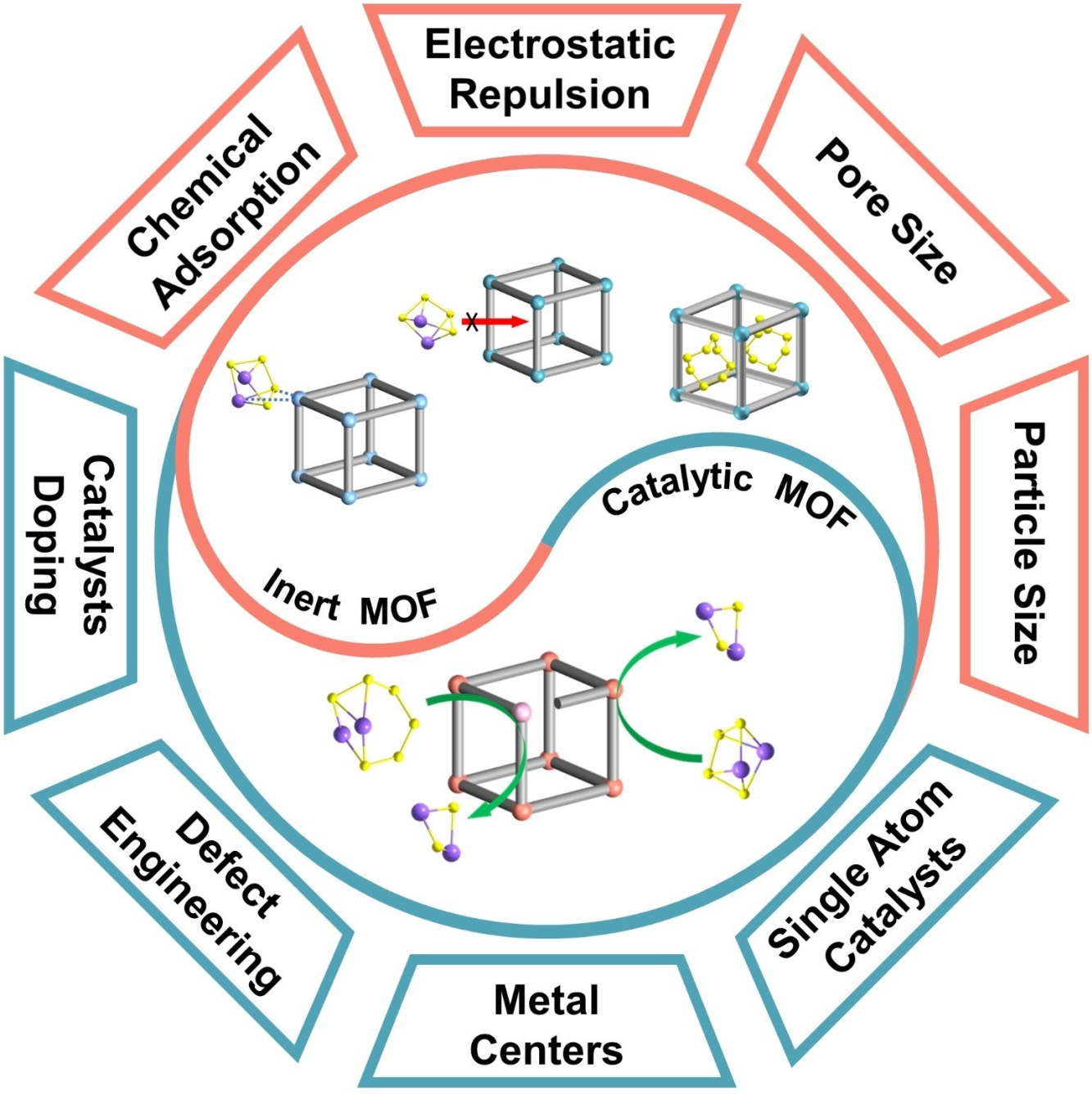

Lithium-sulfur batteries (LSBs) are considered one of the most promising next-generation energy storage devices due to their significant theoretical energy density and high specific capacity of sulfur cathode. However, several critical challenges still must be addressed for practical application. The shuttle effect and sluggish redox kinetics severely impact their performance. Metal-organic frameworks (MOFs) have garnered significant interest attributed to their high structural tunability. Their ability to nano-confine lithium polysulfides (LiPSs) can be precisely controlled at the molecular level by regulating metal centers and organic ligands, thereby suppressing the shuttle effect and improving the electrochemical performance of LSBs. This review summarizes the nano-confinement effects of MOFs in LSBs, and the discussion is divided into the selective confinement, repulsion, and nano-confined adsorption by inert MOFs, as well as nano-confined catalysis facilitated by catalytically active MOFs. Furthermore, the existing challenges and future prospects for application of MOFs in LSBs are proposed.

1. Introduction

Lithium-sulfur batteries (LSBs) have garnered considerable interest in both the scientific community and industry due to their promising attributes, including their high theoretical specific capacity, cost-effectiveness, and the environmental friendliness of sulfur cathodes, positioning them as strong candidates for the next-generation energy storage systems.[1] The cathode of LSBs comprises of elemental sulfur (S_8), while lithium metal serves as the anode material. These batteries exhibit a remarkable theoretical specific capacity of 1675 mAh g^{-1} and an ultrahigh theoretical energy density of 2600 Wh kg^{-1}, surpassing currently available secondary batteries with oxide cathodes.[2] Furthermore, the environmental friendliness and abundant availability of S_8 on Earth augur well for practical LSB applications.[3]

However, several challenges must be overcome for the commercialization of LSBs. The low electronic conductivity of S_8 and the solid discharge products Li_2S_2/Li_2S significantly hinder electron and ion transport within the cathode, leading to underutilization of the active material, particularly at high sulfur loadings.[4] Additionally, the inevitable volume change of approximately 80 % during discharge/charge cycles, caused by the density disparity between S_8 and Li_2S, results in continuous expansion and contraction of the electrode during long-term cycling, ultimately leading to electrode material degradation and battery failure.[5] Another significant issue is the migration of soluble lithium polysulfides (LiPSs) from the cathode, which can diffuse through the separator to the anode, and react with lithium metal. This process leads to the irreversibly loss of active materials. The most critical issue is the sluggish conversion reaction from S_8 to LiPSs and from LiPSs to Li_2S during the discharge process.[6] Wherein, the transformation from LiPSs to Li_2S is considered the rate-limiting step in the sulfur reduction reaction (SRR) due to a significant energy barrier.[7] The slow kinetics of this process cause the accumulation of LiPSs in the electrolyte, resulting in severe shuttle effects and irreversible deposition of discharge product Li_2S on the lithium electrode, significantly diminishing available active material, and thereby leading to rapid capacity decay and poor cycling performance.

To address these issues, extensive researches have been conducted, focusing on the use of sulfur host, functional design of membranes, and protection of the metal anode.[8] In the early stage, carbon materials such as mesoporous carbon,[9] graphene,[10] carbon nanotube (CNT)[11] were developed to enhance the electron conductivity and physically encapsulate LiPSs to mitigate their insulation properties.[12] However, the interaction between nonpolar carbon materials and LiPSs remain insufficient, which is hard to tackle the shuttle effect. Subsequently, polar materials such as heterogeneous atoms-doped carbon and metal compounds/carbon composites were explored for their ability to offer active sites for LiPS adsorption via chemical interactions. Additionally, metal compounds can provide catalytic sites to accelerate the kinetics of LSBs.[13] Nevertheless, the limited number of active sites on these materials are still inadequate for suppressing the shuttle effect, and their chemical tunability remains constrained, limiting their multifunctional potential.

Metal-organic frameworks (MOFs), also known as porous coordination polymers, are hybrid materials formed through the self-assembly of organic ligands with metal ions or clusters.[14] In recent years, MOFs have garnered significant attention and been extensively investigated across various fields such as gas adsorption, drug delivery, catalysis, and energy storage, facilitating the design of functional materials via host-guest chemistry.[15] In the context of LSBs, researchers have conducted comprehensive chemical modifications and host-guest designs on MOFs to achieve a wide range of functionalities.[16] MOFs can serve as efficient ionic sieve, selectively blocking larger sulfur species from penetrating their pores while allowing smaller lithium ions to pass through with properly tuned pore sizes, like ZIF-8,[17] HKUST-1,[18] and Y-FTZB.[19] Additionally, electrostatic repulsion between functional groups and polysulfides can further prevent their diffusion. MOFs with abundant polar sites can chemically adsorb and anchor LiPSs, thus mitigating the shuttle effect.[20] For example, Geng et al.[21] developed an Al/Cu-MOF with sulfiphilic Cu^{2+} which can effectively immobilize LiPSs and suppress their dissolution. Moreover, metal centers and organic ligands within

[a] J. Weng, H. Lu, Q. Zeng, Y. Xiao, J. Yang, J. Rong, Q. Zhang, S. Huang
Guangzhou Key Laboratory of Low-Dimensional Materials and Energy Storage Devices, School of Materials and Energy, Guangdong University of Technology, 510006 Guangzhou, China
E-mail: qzhangmse@gdut.edu.cn
smhuang@gdut.edu.cn
[b] Q. Zhang
State Key Laboratory of Silicon and Advanced Semiconductor Materials, Zhejiang University, 310027 Hangzhou, China
[c] S. Huang
School of Chemistry and Materials Science, Hangzhou Institute for Advanced Study, University of Chinese Academy of Sciences, 310024 Hangzhou, China

MOFs can be tailored to offer catalytically active sites, accelerating the conversion of sulfur species.[22] The post-synthetic modification (PSM) method provides more possibilities for the chemical designability of MOFs,[23] such as ligand exchange, ion exchange and catalyst encapsulation further enhance MOFs' chemical versatility and catalytic activity (Figure 1).[24] Compared to carbon materials, the interactions between metal centers/organic ligands in MOFs and LiPSs are more effective at mitigating the diffusion of LiPSs. Furthermore, the porous structure of MOFs provides a greater number of active sites than carbon materials that are either combined with metal compounds or doped with heteroatoms.[25] Importantly, the high chemical tunability of MOFs enables the rational design of materials with specific structures and functionalities (Figure 2).

While previous research primarily focused on the selective confinement and nano-confined adsorption of MOFs for LiPSs, the accumulation of LiPSs on the cathode side persists due to the sluggish kinetics of multiphase conversion, eventually leading to shuttling to the anode side. Consequently, there is growing research interest in improving the redox reaction kinetics of LiPSs by employing MOFs with catalytic activity (Figure 3).[18,19,26]

Over the past decade, numerous studies have explored various applications of MOFs in LSBs. Several reviews have summarized the specific uses of MOFs in LSBs and tailored chemical interactions.[27] However, the nano-confinement effect remains insufficiently summarized and analyzed. This review provides a systematic overview of the nano-confinement effects of MOFs in LSBs It focuses on two main aspects, including nano-confinement effects to impede the diffusion of LiPSs and boost the conversion of intermediates. Firstly, we highlight the advantages of MOFs in LSBs applications. Subsequently, we explore various specific applications of MOFs in LSBs, including selective confinement, repulsion, and nano-confined adsorption by inert MOFs, and nano-confined catalysis facilitated by catalytically active MOFs. Finally, the remaining challenges and prospects for designing effective MOFs for advanced LSBs are proposed.

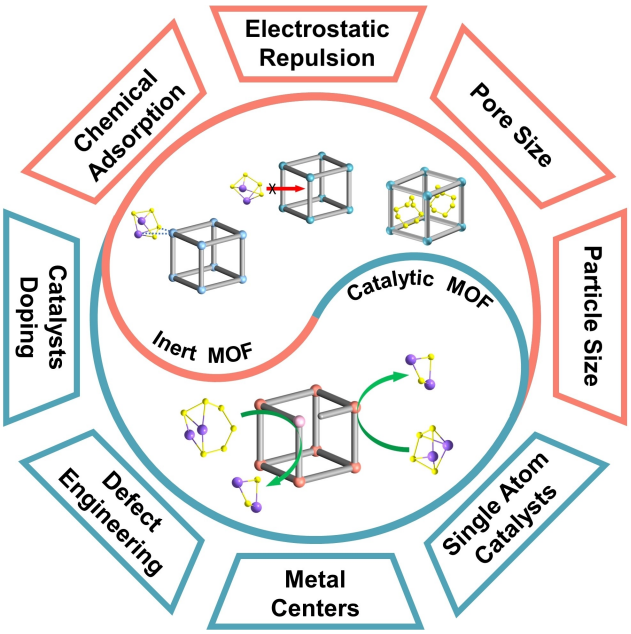

Figure 1. Schematic diagram of MOFs applied in LSBs.

2. Advantages of MOFs for Application in LSBs

Metal centers and organic ligands are fundamental components of MOFs, enabling the construction of open porous crystalline frameworks through reticular coordination. MOFs are promising for the adsorption and catalytic conversion of LiPSs in LSBs due to their tunable structures and abundant active sites. They offer potential benefits as interlayers or separators to mitigate the shuttle effect of LiPSs by: (i) providing a uniform and adjustable

Jingqia Weng received his B.S. degree in New Energy Materials and Devices from Guangdong University of Technology in 2023. He is currently pursuing his Master's degree in Guangdong University of Technology under the supervision of Dr. Qi Zhang. His research interests focus on the application of metal-organic frameworks in lithium-sulfur batteries.

Qi Zhang earned his Ph.D. in Materials Science and Engineering from Zhejiang University in 2017, under the supervision of Prof. Guodong Qian. During 2015–2016, he also conducted research as a joint Ph.D. student at the Institute Lavoisier in France, working with Prof. Christian Serre. He is currently an associate professor at the School of Materials and Energy, Guangdong University of Technology. His research focuses on the design of porous materials, including MOFs, COFs, and HOFs, with applications in advanced energy storage devices.

Prof. Shaoming Huang is currently a professor in Hangzhou Institute for Advanced Study, he is also the director of Collaborative Innovation Center of Advanced Energy Materials at Guangdong University of Technology. He received his B.S. and M.S. degrees in Physical Chemistry from Hangzhou University in 1985 and PhD degree in Chemistry from Nankai University in 1991. His research interests mainly focus on the synthesis and properties of nanostructured carbons and their applications in energy conversion and storage devices.

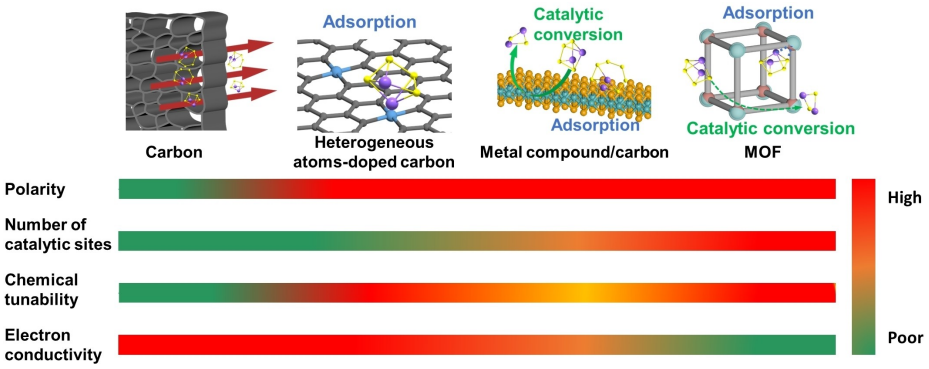

Figure 2. Comparison between MOFs and other traditional materials used in LSBs.

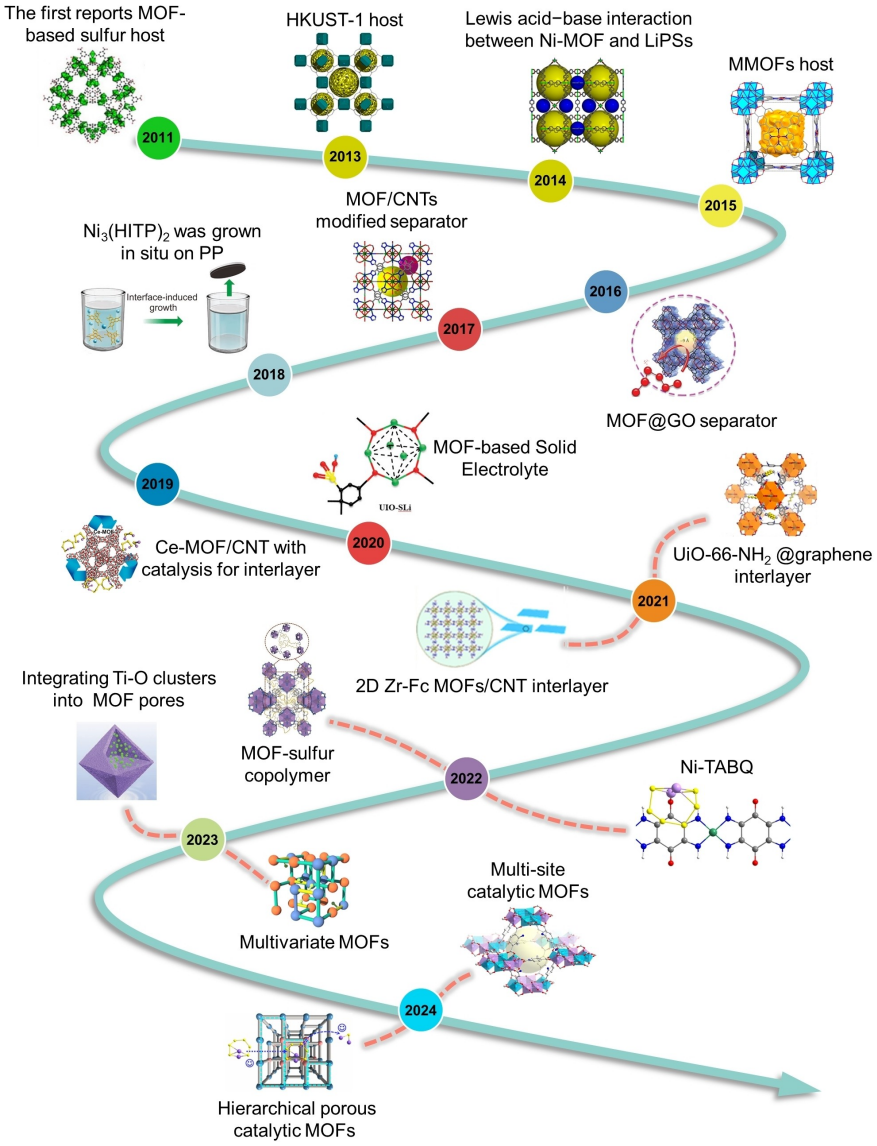

Figure 3. Development progress of MOFs in LSBs. Reprinted with permission.[18,19,26] Copyright 2011, 2013, 2014, 2015, 2017, 2019, 2024, American Chemical Society. Copyright 2016, Nature Publishing Group. Copyright 2018, 2020, 2022, 2023, 2024, Wiley-VCH. Copyright 2021 Springer Nature. Copyright 2021, 2022, 2023 Elsevier.

pore structure that physically restricts and sieves LiPSs; (ii) offering numerous tunable polar sites for chemical adsorption to confine of LiPSs; (iii) promoting the rapid conversion of LiPSs through engineered metal centers and organic ligands with

catalytic activity. (iv) porous structure serving as an ion sieve, promoting a consistent Li^+ flux during the reaction process.[28] Furthermore, MOFs demonstrate considerable potential as sulfur host in LSBs due to their structural and functional diversity. Their uniform pore structure facilitates the even distribution of sulfur, and some electrolytes can be stored within the porous frameworks, acting as secondary electrolyte sources and reducing irreversible electrolyte consumption during long-term cycling. MOFs also exhibit chemical polarity, unlike porous carbon materials, allowing them to chemically adsorb LiPSs and confine them within their pores. The abundant polar functional groups enhance the binding between polysulfide ion and Li^+, ensuring a uniform electric field distribution.[29] Moreover, more favorable host-guest interaction can be obtained by regulating the synergistic effect between catalytic centers and bulk structure, therefore improving the catalytic efficiency.[30] In a word, MOFs exhibit significant potential for application in LSBs.

3. Inert MOFs for LSBs

3.1. Size Effect Leaded Selective Confinement

MOFs feature a unique and tunable porous structure that provides a high specific area and adjustable pore sizes. This property enables MOFs to selectively block larger sulfur species from penetrating their pores while allowing smaller lithium ions to pass through, primarily due to pore size effect. The size effect leaded selective confinement allows the selective and confined transport of Li^+ through nano-channels, realizing suppressing of shuttle effect. In this section, the researches on size effect leaded selective confinement of MOFs in LSBs are discussed. Table 1 provides a comprehensive summary.

MOFs possess a large surface area and highly ordered pores with tunable porosity, making them suitable as ionic sieves to impede the shuttle of polysulfide ions. Bai et al.[18] utilized HKUST-1 with a pore size of ~9 Å to construct a MOF@GO separator. During the cycling process, the MOF@GO separator not only acts as an ionic sieve to prevent polysulfides shuttling but also permits lithium ions to pass through. The LSBs with this MOF@GO membrane exhibit a low-capacity decay rate of 0.019% per cycle after 1500 cycles. In another work, they developed a Zn(II)-MOF based MOF@GO separator which also functions effectively as an ionic sieve with great performance.[31]

Through a systematically comparison of MOFs with different pore sizes (ZIF-7 (Ms-2.9), ZIF-8 (Ms-3.4), and CuBTC (Ms-9.0)), Chang et al.[32] investigated the "pore size effect" of MOFs interlayers within LSBs. They observed that MOFs with relatively larger pore sizes tend to trap LiPSs more seriously due to the interaction between LiPSs and metal sites in MOFs, resulting in initial "sulfur loss" and low coulomb efficiency. On the contrary, reducing pore sizes of MOFs can alleviate trapped LiPSs but may hinder Li^+ transport kinetics, leading to severe polarization.

Tian et al.[33] introduced a simple method for synthesizing thin molecular-layered copper-based MOFs (Cu_2(CuTCPP)) nanosheets and demonstrated their efficacy in fabricating functional separators with MOFs interlayer via vacuum filtration of the ultra-thin MOFs nanosheet suspension on PP separators. Compared to pristine PP separators, the Cu_2(CuTCPP) nanosheet-modified separators with uniform micropores and a dense structure can significantly reduce the shuttle effect of LiPSs. The directed assembly of Cu_2(CuTCPP) nanosheets on the large-pore PP separator forms an ideal physical barrier, inhibiting the migration of LiPSs, while the oriented pores ensure the optimal pathway for Li^+ transport.

However, relying solely on the size effect leaded selective confinement with MOFs is insufficient to impede the diffusion of LiPSs, primarily due to the relatively weak interactions between MOFs and LiPSs. To effectively address the shuttle effect, it is crucial to strengthen these interactions.

3.2. Chemical Interaction Leaded Repulsion

In addition to optimizing pore size, MOFs can also suppress the shuttling of LiPSs via electrostatic repulsion between the negative charged groups on ligands and polysulfides. Chiochan et al.[26g] prepared a solid-state electrolytes (SSEs) by grafting lithium sulfonate ($-SO_3Li$) groups onto UiO ligand. While the pore size of MOF can inhibit the penetration of polysulfides, it allows the transport of Li^+. Furthermore, the presence of $-SO_3^-$ on the MOF induces repulsion against polysulfides while enhancing Li^+ transport. The UIOLi SSE demonstrated a capacity fading rate of 0.06% per cycle after 250 cycles.

Table 1. Inert MOFs with selective confinement effect used in LSBs.

MOFs materials	Application	Pore Size	Cycling performance [discharge capacity after cycling (mAh g−1)/rate/cycles]	Refs.
MOF@GO	Separator	9 Å	~880/1 C/1500	[18]
Y-FTZB	Interlayer	9 Å	452/0.25 C/300	[19]
ZIF-7	Interlayer	2.9 Å	~720/0.5 C/500	[32]
ZIF-8	Interlayer	3.4 Å	~590/0.5 C/500	[32]
CuBTC	Interlayer	9 Å	~770/0.5 C/500	[32]
HKUST-1	Separator	9 Å	~470/2 C/2000	[8d]
Cu_2(CuTCPPP)	Interlayer	10 Å	604/1 C/900	[33]
Mg-MOF-74	Separator	10.2 Å	837.8/0.1 C/200	[36]

Similarly, Wang et al.[34] designed a mixed-matrix membrane (MMM) using UiO-66-SO_3Li and drew the same conclusion with Chiochan's work.

Lin and co-workers[35] prepared a heavily lithium sulfonate-rich MOF (UiO-66$(SO_3Li)_4$) as interlayer to prevent the shuttle of polysulfides. The UiO-66$(SO_3Li)_4$ shows a stronger electrostatic repulsion than those with one or two $-SO_3Li$ groups. Moreover, it creates ionic pathways for the fast transport of Li^+.

3.3. Chemical Interaction Leaded Nano-Confined Adsorption

The tunable structure of MOFs offers a versatile platform for mitigating the shuttle effect of LiPSs and enhancing the performance of LSBs. To achieve enhanced the nano-confinement of LiPSs through chemical interactions, designing MOFs with exposed metal centers and polar functionalized ligands is considered an effective strategy. Compared to physical selective confinement, nano-confined adsorption can more effectively suppress the shuttle effect, thereby leading to superior electrochemical performance. Table 2 provides a comprehensive summary.

3.3.1. Chemical Interaction Leaded Nano-Confined Adsorption in Interlayer/Separator

Zang et al.[26e] using $Ni_3(HITP)_2$ to construct a crack-free microporous membrane on PP separator. The narrow size of its uniform 1D microporous channels act as physical barrier to block the diffusion of LiPSs, while the polar sites can effective adsorb LiPSs. As a result, the LSBs with the light-weight interlayer exhibited a reversible discharge capacity of 589 mAh g^{-1} at 5 C, and a long-term cycling stability (716 mAh g^{-1} after 500 cycles).

Wu et al.[37] designed a CNT@ZIF functional interlayer to capture the dissolved polysulfides. The MWCNTs network can physically restrict the diffusion of LiPSs while the ZIF-8 distributing on MWCNTs inhibiting the shuttle via Lewis acid-base interaction between Zn sites and polysulfides.

Guo et al.[26h] systematically studied the interactions between different functionalized MOFs and LiPSs and prepared an ordered interlayer by assembling UiO-66-NH_2 on graphene. The UiO series of MOFs offers extensive chemical tunability by modifying functional groups (–OH, $–NH_2$, and –COOH) while maintaining similar structures, enabling study of their influence on their LiPSs constraint and electrochemical performance. Adsorption experiments demonstrated that all functionalized MOFs, namely UiO-66-2OH, UiO-66-COOH, and UiO-66-NH_2, exhibited stronger adsorption capability compared to bare UiO-66, with UiO-66-NH_2 demonstrating the highest affinity for Li_2S_6. Enhanced adsorption was attributed to the chemical interactions between functional groups in MOFs and LiPSs. Additionally, the arrangement of UiO-66-NH_2 particles between graphene sheets facilitated a densely packed structure, guiding LiPSs to diffuse only along the interlayer space of the graphene sheets, extending their diffusion path and being captured by UiO-66-NH_2 during the diffusion process (Figure 4a). Consequently, compared to batteries with a bare separator, the ordered UiO-66-NH_2@graphene interlayer increased the initial discharge capacity of the battery by 28.98% at 1.0 C and reduced the capacity decay rate remarkably from 0.10% to 0.067% per cycle.

3.3.2. Chemical Interaction Leaded Nano-Confined Adsorption in Host

Zheng et al.[26c] reported a microporous Ni-MOF with a pore size of 1.38 nm as a sulfur host for LSBs. The Ni(II) centers within Ni-MOF act as Lewis acidic sites, interacting with the S_x^{2-} in LiPSs as Lewis bases. This interaction enables effective capture of LiPSs, thereby inhibiting the shuttle effect. To further investigate the interaction mechanism between transition metal ions and LiPSs, they also prepared Co-MOF by substituting Co(II) for Ni(II) center ions. Despite Co-MOF exhibited better conductivity

Table 2. Inert MOFs with nano-confined adsorption ability used in LSBs.

MOFs materials	Application	Adsorption sites	Cycling performance [discharge capacity after cycling (mAh g^{-1})/rate/cycles]	Refs.
PSS@HKUST-1	Interlayer	Metal centers	755/0.5 C/500	[38]
Ni-MOF/MWCNT	Interlayer	Metal centers	1183/0.2 C/300	[39]
CNT/ZIF-30	Interlayer	Metal centers	870.3/0.2 C/100	[37]
$Ni_2(HITP)_3$	Interlayer	Metal centers	716/1 C/500	[26e]
MIL-125(Ti)	Interlayer	Organic ligands	726/0.2 C/200	[40]
B/D MOF-Co	Separator	Metal centers	~450/1 C/600	[41]
UiO-66-NH_2@graphene	Interlayer	Organic ligands	590/1 C/500	[26h]
ZIF/CNF	Interlayer	Metal centers	569/1 C/300	[42]
ZIF-67	Interlayer	Metal centers	816/3 C/300	[20]
Ni-MOF	Host	Metal centers	611/0.1 C/100	[26c]
MOF-525(Cu)	Host	Metal centers	700/0.5 C/200	[26d]
Al/Cu-MOF	Host	Metal centers	~500/1 C/200	[21]
MIL-96-Al	Host	Metal centers	389/0.1 C/200	[43]

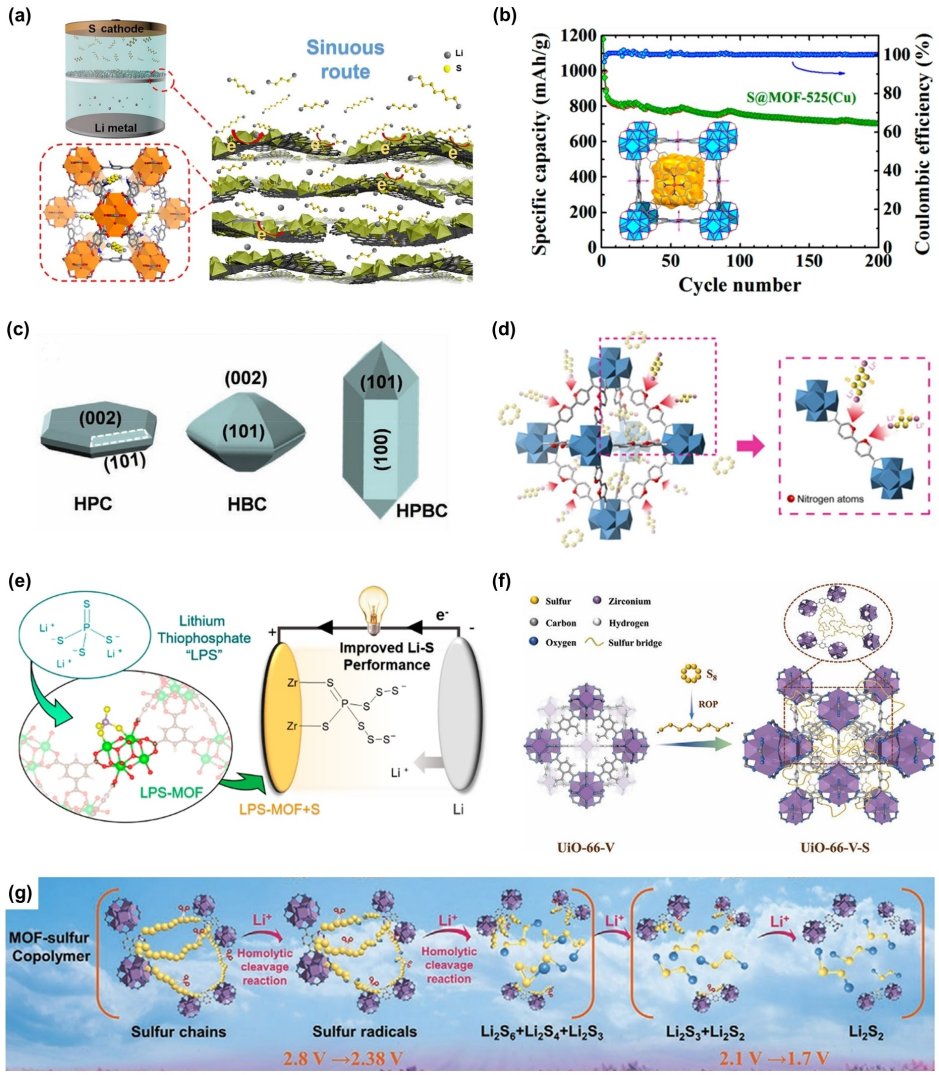

Figure 4. (a) Schematic illustration of the design of chemical interaction and microstructure of the interlayer constructed with UIO-66-NH_2 and graphene. Reprinted with permission.[26h] Copyright 2021 Springer Nature. (b) Schematic diagram and cycle performance of S@MOF-525(Cu). Reprinted with permission.[26d] Copyright 2015 American Chemical Society. (c) Different crystal shapes of MIL-96-Al. Reprinted with permission.[43] Copyright 2022 Wiley-VCH. (d) Schematic illustration of the chemical interactions between nitrogen atoms in nMOF-867 and LiPSs. Reprinted with permission.[44] Copyright 2016 Springer Nature. (e) Mechanism of LSBs utilizing Zr-MOFs as sulfur host. Reprinted with permission.[16b] Copyright 2019 American Chemical Society. (f) Schematic diagram of the synthesis route of UiO-66-V-S. g) Transformation processes of sulfur species in UiO-66-V-S cathode. Reprinted with permission.[26j] Copyright 2022, Wiley-VCH.

than Ni-MOF, its cycling stability as a sulfur host for LSBs was inferior to Ni-MOF, which may be due to the weaker coordination between Co(II) and LiPSs. Research has shown that Cu^{2+} has a strong affinity for sulfur.[45] Wang et al.[26b] utilized HKUST-1 combined with sulfur to obtain HKUST-1/S cathodes for LSBs. The pore structure of HKUST-1 effectively confines sulfur species, while the open sites of Cu^{2+} further enhance the immobilization of LiPSs, thereby improving the cycle stability. Similarly, experiments using a zirconium-metalloporphyrin framework (MOF-525(Cu)) as a sulfur host reported by Wang et al.[26d] demonstrated effective adsorption of LiPSs and dissolution inhibition. Because each incorporated Cu^{2+} provided two Lewis acid sites, enhancing the binding energy between the MOFs and LiPSs, S@MOF-525(Cu) delivered a high reversible capacity of 704 mAh g^{-1} after 200 cycles (Figure 4b).

The shape and particle size of MOFs influence the exposure of specific crystal planes, which in turn affects their adsorption capacity for LiPSs. Geng and co-workers[43] prepared various shapes of MIL-96-Al, including hexagonal platelet crystals (HPC), hexagonal bipyramidal crystals (HBC), and hexagonal prismatic bipyramidal crystals (HPBC) (Figure 4c). Density functional theory (DFT) calculations and electrochemical experiments revealed that the HBC shape with highly exposed (101) planes can effectively adsorb LiPSs. Besides, MOFs with smaller size of the HBC shape exhibit faster Li^+/electron transfer rate and better cyclability.

Functionalizing MOF ligands is another strategy to boost chemical adsorption capacity for LiPSs. Park et al.[44] used in situ spectroelectrochemical measurements to demonstrate that sp^2 nitrogen atoms within the ligands of nMOF-867 can encapsu-

late LiPSs, thereby preventing their dissolution into the electrolyte during discharge/charge cycles (Figure 4d). This encapsulation mechanism was further confirmed by observed shifted in FTIR spectra of C=N and C–N bonds, as well as XPS spectra showing Li–N bonds from nMOF-867. As a result, cathodes fabricated using nMOF-867 exhibited excellent capacity retention (500 cycles with a capacity loss of 0.027% per cycle). Baumann et al.[16b] reported the capture of LiPSs using lithium thiophosphate encapsulated in Zr-MOFs. By anchoring the PS_4^{3-} group to the porous skeleton of the MOFs, reversible formation of S–S/Li–S bonds with LiPSs during cycling was facilitated, effectively preventing the adverse dissolution of LiPSs and thiophosphates into the electrolyte (Figure 4e). Incorporating thiophosphates demonstrated improved capacity and retention at various rates.

MOFs-sulfur copolymerization provides a novel approach to mitigate the dissolution and diffusion of LiPSs, offering new possibilities for designing advanced sulfur hosts.[46] In the MOFs-sulfur copolymerization cathode, the LiPSs are permanently immobilized via strong covalent bonds formed during electrochemical reactions, achieving enhanced sulfur utilization and exceptional electrochemical performance. In general, heating S_8 at 160 °C initiates a ring-opening reaction to form linear sulfur.[47] And then copolymerisation of linear sulfur with hosts can be achieved by introducing MOFs hosts. These linear sulfur species are linked to MOFs by covalent bonds, mainly including alkene/carbonyl (C=C/C=O), and sulfydryl (–SH).[48] Liu et al.[16a] employed thiol-modified CNTs@UIO-66 as the host, and synthesized a cathode material (CNTs@UIO-66/S) via covalently linking sulfur to CNTs@UIO-66-SH. XPS analysis confirmed the formation of S–S bonds and the disappearance of S–H bonds in CNTs@UIO-66/S, indicating that S_8 reacts with the –SH groups of UIO-66-SH to form C–S bonds, thereby preventing the dissolution of LiPSs. CNTs@UIO-66/S showed high discharge capacity and excellent cyclic stability (remaining at 80.19% after 900 cycles at 2 C), attributed to the anchoring of LiPSs on the surface of UIO-66 during the electrochemical reaction. Inspired by their work, Zeng et al.[26j] designed and synthesized a MOFs-sulfur copolymer (CNTs@UiO-66-V-S), where sulfur chains were co-polymerized with vinyl-functionalized MOFs (UiO-66-V) (Figure 4f). This covalently attachment of sulfur to the host material improved sulfur stability within the carrier. Compared to physically mixed sulfur electrodes (CNTs@UiO-66-V/S), CNTs@UiO-66-V-S exhibited significantly enhanced electrochemical performance. Specifically, the discharge capacity at 3 C increased by 86.7%. In terms of cycling stability, it sustained 1000 cycles at both 1 C and 3 C rates, maintaining a capacity of 609 mAh g^{-1} after 1000 cycles at 1 C with a capacity decay rate of 0.028% per cycle. Unlike traditional stepwise redox reactions during discharge, the S–S bonds in polymer sulfur chains underwent scission reactions, generating free radicals of varying lengths. These free radicals reacted simultaneously with Li^+ and e^-, producing three types of LiPSs: Li_2S_6, Li_2S_4, and Li_2S_3 (Figure 4g). During this process, long-chain LiPSs were anchored to the MOFs framework, limiting their dissolution into the electrolyte, and effectively suppressing the shuttle effect. The free radical reaction mechanism facilitated the conversion of LiPSs to Li_2S_2, reducing the residence time of LiPSs and improving the performance of LSBs.

4. Catalytically Active MOFs for LSBs

Solely relying on size effects and nano-confined adsorption of MOFs to confine LiPSs is insufficient to suppress the shuttle effect, due to sluggish redox kinetics during LiPSs conversion. This limitation leads to continuous accumulation of LiPSs in the electrolyte and restricts the utilization of active materials, especially under high sulfur loading and low electrolyte content. The adjustable metal atom centers and organic ligands within MOFs offer an opportunity for achieving nano-confined catalysis through rational design to accelerate the conversion of LiPSs, therefore mitigating the shuttle effectively. Table 3 summarizes various catalytically active MOFs for LSBs.

4.1. Pristine Catalytic MOFs

4.1.1. Pristine Catalytic MOFs for Interlayer

Guo et al.[56] utilized the smallest π-conjugated ligand HAB and Ni(II) center to assemble Ni-HAB on CNT, forming Ni-HAB@CNT. The small size of HAB enhances its ability to capture LiPSs and increases the density of active sites (Figure 5a). DFT calculations revealed the unique dsp^2 hybridization endows Ni(II) with planar tetracoordinate structure, minimizing steric hindrance between the active sites and polysulfides, thereby enhancing catalytic activity. Then the random agglomeration of MOF nanoparticles triggered by nano-effect is decreased due to the introduction of CNT substrate, thus exposing more catalytic sites (Figure 5b). When used as an interlayer in LSBs, Ni-HAB@CNT exhibited a capacity attenuation rate of 0.041% per cycle after 500 cycles at 1 C and an areal capacity of 6.29 mAh cm^{-2} under a sulfur loading of 6.5 mg cm^{-2}.

Similarly, Gu et al.[70] introduced another MOF with M-N_4 centers, a 2D conductive MOF ($Co_3(HTIP)_2$) with rich and periodic Co-N_4 catalytic centers as an interlayer material. Systematic calculations and experiments indicated that the functionalized MOF suppresses the diffusion of polysulfide through chemical interactions and promotes the redox reaction via Co-N_4, decreasing the reaction barriers. The LSBs with $Co_3(HTIP)_2$-decorated carbon fiber paper (CFP) as an interlayer showed a low-capacity fading rate of 0.028% at 1 C after 1000 cycles. Moreover, under a high temperature condition of 45 °C they achieved a reversible capacity of 762 mAh g^{-1} and maintained a capacity retention rate of 79.6% after 500 cycles.

A traditional Co-ZIF-9, composed of Co^{2+} as metal center and benzimidazole as ligand, possesses abundant Co catalytic active sites and has been employed as an efficient catalyst.[73] Wu et al.[74] utilized Co-ZIF-9 as an electrocatalytic membrane for LSBs to enhance the electrochemical performance. The blocky Co-ZIF-9 sheets provide a "plane-to-point" mode to expose more pores and active sites in the Interlayer, thus exhibiting a powerful adsorption towards LiPSs. Meanwhile, the

Table 3. Various catalytically active MOFs for LSBs.

MOFs materials	Application	Rate performance [reversible capacity (mAh g^{-1})/rate]	Cycling performance [discharge capacity after cycling (mAh g^{-1})/ rate/cycles/decay rate]	Refs.
Ce-MOF-2/CNT	Interlayer	662.6/4 C	838.8/1 C/800/0.022%	[26f]
PCN@CNT	Interlayer	696/2 C	545/1 C/500/0.067%	[26i]
CSUST-1/CNT	Interlayer	~720/5 C	538/2 C/1200/0.037%	[22b]
D-UiO-66-NH_2–4	Interlayer	840/3 C	~700/3 C/600/0.013%	[49]
Zr-Fc MOF/CNT	Interlayer	757/5 C	~450/1 C/1500/0.027%	[26i]
Bi-MOF-1/rGO	Interlayer	590/3 C	799.8/1 C/1000/0.17%	[50]
MIL-101@CC	Interlayer	635/3 C	655/1 C/500/0.04%	[51]
ZIF-67/SA-PAN	Separator	707/2 C	445/1 C/500/0.089%	[52]
UiO-67-GF	Interlayer	651/5 C	738/1 C/500/0.04%	[53]
$Ti_3C_2T_x$/Ni-Co MOF	Interlayer	660/2 C	~680/1 C/500/0.05%	[54]
Ni-TABQ	Interlayer	487/5 C	820/1 C/1000/0.019%	[26k]
ZIF-B	Interlayer	~980/3 C	630/2 C/1000/0.025%	[55]
MIL-125(Ti)-HT-LE	Interlayer	~750/3 C	882.1/1 C/800/0.024%	[26m]
Ni-HAB@CNT	Interlayer	799/3 C	804/1 C/500/0.041%	[56]
Ni-MOF-74/CNT	Interlayer/anode	732/5 C	741/5 C/1000/0.028%	[57]
MOF@CC	Interlayer	765/5 C	920/0.5 C/100/0.12%	[58]
NiCo-MOF/LDH	Interlayer	640/5 C	950/1 C/200/0.033%	[59]
3DOM ZIF-8	Host	803/2 C	674/2 C/500/0.028%	[60]
2D CoNi MOF	Host	980/3 C	790/1 C/500/0.036%	[61]
Ni-HHTP@CP	Host	892/2 C	910/0.2 C/200/0.165%	[62]
HE PBA	Host	424/1 C	570.9/1 C/200/0.286%	[63]
In-PIA@rGO	Host	429/2 C	519.8/0.5 C/200/0.312%	[64]
ZIF-7–600	Host	511.3/5 C	~680/1 C/500/0.05%	[65]
Ni-MOF-1D	Host	575/8 C	588/3 C/1000/0.018%	[66]
MOF-808-Zn	Host	599/2 C	630/1 C/300/0.018%	[67]
D-MOF-Cu	Host	716.1/5 C	695.9/1 C/1000/0.03%	[68]
MOF-TOC	Host	740.3/3 C	805/1 C/500/0.031%	[26l]
ZnCo-MOF	Host	552/2 C	668/0.5 C/300/0.023%	[69]

plentiful Co and N catalytic sites accelerate the redox reaction kinetics of LiPSs. The resulting Co-ZIF-9/CNT interlayer demonstrated excellent rate capacities of 1011 and 817 mAh g^{-1} at 1 C and 3 C, respectively. Furthermore, it also obtained a stable cyclability with a fading rate of 0.019% over 1000 cycles at 1 C.

Cerium Oxides have proven effective in immobilizing and catalyzing the conversion of LiPSs.[75] Hong et al.[26f] combined Ce-MOF-808 with CNTs to form Ce-MOF-2/CNT utilized as the separator coating for LSBs. DFT calculation and electrochemical test indicate that Ce(IV) could strongly immobilizes polysulfides and enhances reaction kinetics (Figure 5c). This is because Ce-MOF-2/CNT with a large specific surface area and coordination-unsaturated Ce(IV)-cluster nodes could quickly adsorb the polysulfides and effectively promote their conversion. They also verify the impact of the coating thickness on the LSBs performance, revealing challenges in polysulfide blockage with excessively thin coatings. The LSBs with Ce-MOF/CNT coating separator achieved a capacity decay rate of only 0.022% per cycle after 800 cycles at 1 C.

Su et al.[76] synthesized another Ce-MOF (Ce-UiO-66-NH_2) as a multifunctional interlayer for LSBs. The Ce-MOF/Super-P coating separator can inhibit the shuttle of LiPSs via electrostatic repulsion of amino group and Lewis acid-base interactions between LiPSs and Ce-MOF. Most importantly, metal sites within Ce-MOF further promote the conversion of polysulfide, significantly suppressing the shuttle effect. Therefore, the Ce-

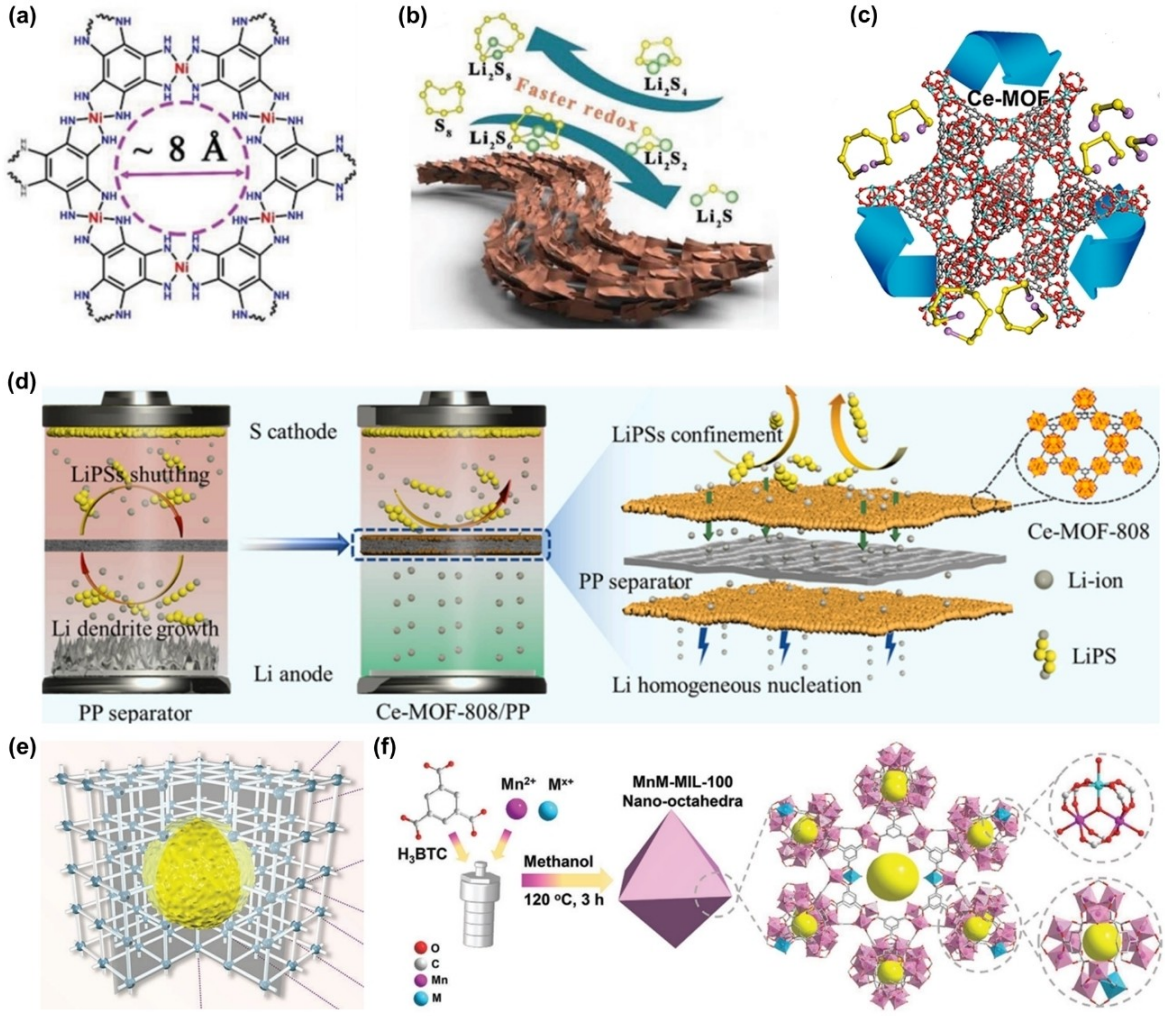

Figure 5. (a) The structure of Hi-HAB (b) Schematic illustration of the sulfur transformation process on Ni-HAB@CNT. Reprinted with permission.[56] Copyright 2023, Wiley-VCH. (c) Scheme depicting Ce-MOF-2 catalyzing the conversion of polysulfides. Reprinted with permission.[26f] Copyright 2019, American Chemical Society. (d) Schematic of the Ce-MOF-808/PP separator. Reprinted with permission.[71] Copyright 2022, Elsevier. (e) Schematic illustrating the "fish-in-net" encapsulation of sulfur nanoparticles. Reprinted with permission.[30] Copyright 2023, Wiley-VCH. (f) Schematic illustrating the preparation of MnM-MIL-100. Reprinted with permission.[72] Copyright 2021, Wiley-VCH.

MOF/Super-P allowed LSBs to show a low-capacity degradation of 0.09% at 1 C upon 300 cycles. Similarity, Dang et al.[53] developed Ce-UiO-67 modified glass fiber (UiO-67-GF) as a bifunctional separator. Ce-MOF hinder the shuttle effect via adsorption and catalysis for LiPSs, while the abundant O-containing lithophilic groups of UiO-67-GF facilitate uniform deposition of Li^+, restraining Li dendrites growth. As a result, the separator exhibited an excellent cyclability with a capacity fading rate of 0.04% per cycle over 500 cycles at 1 C. In addition, it achieved an areal capacity of 6.0 mAh cm^{-2} under a high sulfur loading of 7.0 mg cm^{-2} with a low electrolyte/sulfur ratio (E/S) 6.0 μL mg^{-1}. In another work, they reported Ce-MOF-808 to functionalize PP separator by *in-situ* growth method.[71] The Ce^{III}/Ce^{IV} redox couple of Ce-MOF-808 facilitates the conversion of LiPSs, while oxygen groups in dicarboxylic acid ligands ensure fast and homogeneous flux of Li^+. Consequently, the PP separators modified by continuous Ce-MOF-808 on both sides play triple roles of adsorption, serving and catalysis towards LiPSs, suppressing the shuttle effect and the growth of Li dendrites (Figure 5d). The LSBs assembled the modified separator indicated an exceptional cycling stability with a low-capacity fading rate of 0.025% at 1 C for 500 cycles and a high-rate performance of 763.5 mAh g^{-1} at 5 C. Even at 7.0 mg cm^{-2} sulfur loading and a low E/S of 6.0 μL mg, the batteries still obtained an areal capacity of 5.9 mAh cm^{-2}.

Wang et al.[77] prepared a Zr-based MOF also belonging to MOF-808 family. The continuous MOF-808 was fabricated on CNT film as a multifunctional interlayer of LSBs, which acting as an ionic sieve to impede LiPSs, facilitate rapid passage of Li^+ and promote redox kinetics. Therefore, the LSBs with this interlayer showed a decay rate of only 0.03% per cycle over 500 cycles at 1 C, maintaining the capacity of 755.5 mAh g^{-1}. Furthermore, the interlayer enabled excellent high-rate performance (869.9 mAh g^{-1} at 3 C and 707.3 mAh g^{-1} at 5 C).

Razaq and co-workers prepared a dual functional bimetallic MOF by introducing dopant Fe into ZIF-8 (Fe-ZIF-8) via a low-

cost synthesis process using H_2O as the only solvent at 35 °C.[78] The Fe sites endowed the MOF with electrocatalytic activity, promoting the conversion of LiPSs. Furthermore, the uniform pore size facilitated even transport and deposition of Li^+, inhibiting the formation of dendrite. Consequently, the LSBs assemble with the Fe-ZIF-8 modified PP separators displayed an initial capacity of 746 mAh g^{-1} at 3 C and a long-term cyclability with a decay rate of 0.06% after 1000 cycles at 0.5 C.

Wang et al.[26i] demonstrated that Zr-Fc MOF can effectively anchor polysulfides due to electrostatic attraction between positively charged open metal sites and electronegative polysulfides, and the formation of firm Li–O bond. To be specific, the electrostatic attraction arises from the uncoordinated Zr–O defects in Zr-Fc MOF and Fc ligands, exposing more positively charged open Zr sites that could trap polysulfides with high-efficiency. Moreover, electrochemical experiments confirmed its strong catalytic ability towards different polysulfides intermediate. The LSBs with Zr-Fc MOF/CNT interlayers exhibited a stable long-term cyclability with ultralow capacity decay rate of 0.027% over 1500 cycles at 1 C under sulfur loading of 4.11 mg cm^{-2}.

Xiao et al.[26k] introduced the concept of effectively catalyzing multistep LiPSs conversion using single catalyst by integrating dual catalytic centers (Ni-N_4 and quinone) within a MOF (Ni-TABQ). The dual centers in Ni-TABQ can capture Li_2S_6 and realize stronger adsorption capabilities compared to single-center configurations. Furthermore, electrochemical tests indicated that the catalytic activity of Ni-N_4 center for the reduction of S_8 to LiPSs is better than quinone, while quinone is superior in catalyzing the reduction of LiPSs to Li_2S/Li_2S_2. Thanks to the synergistic effect of dual catalytic centers, the LSBs with Ni-TABQ interlayer exhibited excellent cycling performance (821 mAh g^{-1} after 1000 cycles at 1 C).

4.1.2. Pristine Catalytic MOFs for Host

MOFs formed by metal centers and π-conjugated ligands exhibit excellent conductivity attributed to π-d conjugation effect.[79] Yang et al.[66] introduced a 1D π-d conjugated MOF (Ni-MOF-1D) as a highly conductive sulfur host. According to calculation results, the electrons from polysulfide anions can transfer to the unfilled d orbital of Ni sites in Ni-MOF-1D, forming Ni–S bond. Additionally, the interaction between Li in LiPSs and N in Ni-MOF-1D facilitates chemical bonding via Lewis acid-base interaction. Furthermore, the reduction of sulfur on Ni-MOF-1D is more favorable in thermodynamics compared to carbon materials. This also has been proved by a series of electrochemical experiment. The LSBs with Ni-MOF-1D as sulfur host material exhibited a discharge capacity of 588 mAh g^{-1} with an average 0.018% degradation per cycle over 1000 cycles at 3 C.

Prussian blue analogues (PBAs) are a special class of MOF, possessing numerous exposed metal centers serving as Lewis acid sites and open framework structures capable of confining LiPSs, making them promising for the application of LSBs.[80] Shen and co-workers[81] developed a 3D "necklace"-like microstructure PB/CNT hybrid as the sulfur host including defective PB. The interaction and catalytic activity of PB towards LiPSs are enhanced by the increased vacancy sites of $[Fe(CN)_6]$. Specifically, a surface $[Fe(CN)_6]$ vacancy is generated by removing one Fe(II) atom and five C≡N ligands, allowing two sulfur atoms to coordinate with the exposed Fe(III).The configuration strengthen the interaction between LiPSs and MOFs, stretching and weakening the S–S bond, thereby improving the catalytic activity towards LiPSs. The defective PB embedded within intertwined CNT networks as the host material exhibited good performance with a high initial capacity (1457 mAh g^{-1} at 0.2 C) and stable cyclability (low degradation rate of 0.052% after 1000 cycles). Meng et al.[63] successfully synthesized a range of PBAs from binary to high-entropy through a simple coprecipitation method at room temperature. Systematic experiments revealed that high-entropy PBA (HE-PBA) effectively immobilize LiPSs and enhance their conversion. As a result, the LSBs with HE-PBA-S cathode exhibited superior electrochemical performance. Additionally, they developed various nanocubic metal oxides from binary to senary by using PBAs as sacrificial precursors, thus advancing the development of multifunctional host materials.

Rana et al.[82] reported an antiferroelectric perovskite DMAZF MOF with Zn sites and tuned porosity to serve as sulfur host. The nanoporous structure simultaneously physically blocks LiPSs anions and facilitates Li^+ transport. Furthermore, Zn sites not only adsorb polysulfides but also promote electrochemical kinetics of nucleated polysulfide. As a result, the DMAZF MOF supported by CNTs delivered excellent electrocatalytic properties. The DMAZF/CNTs/sulfur electrodes displayed initial capacities of 1260 mAh g^{-1} and 1007 mAh g^{-1} at 0.05 C and 0.1 C respectively with a sulfur loading of 5 mg cm^{-2}. Even under a sulfur loading of 7 mg cm^{-2}, they exhibited cycling performance with a capacity fading rate of 0.12% at 0.5 C after 500 cycles.

Meng et al.[61] proposed a bimetallic MOF to improve electrochemical performance, focusing on the synergistic effect between two different catalytic centers. They found that Ni-MOF effectively catalyzes the liquid-liquid process that could ensure the complete conversion of the long-chain polysulfides, while Co-MOF facilitates the liquid-solid step which is the consumption of the soluble polysulfides and the nucleation of Li_2S. By integrating these two metals into one framework, CoNi-MOF exhibited a low-capacity decay rate of 0.036% per cycle after 500 cycles at 1 C. This is due to charge redistribution between Ni and Co via oxygen bridges in MOF structure, facilitating tandem catalysis of two-step reaction. The catalytic activity of Ni in reducing polysulfides to Li_2S had been further confirmed by Li et al.[83] Moreover, they suggested that catalytic activity will improve with the increasing exposed adsorption sites by comparing the electrochemical performance of 2D-Ni-MOF/CNTs with 3D/-Ni-MOF/CNTs.

In another work, Ren et al.[30] introduced a "fish-in-net" concept to encapsulate sulfur into catalytic MOFs (Figure 5e). To be specific, the bimetallic Co/Ni MOFs act as shell around the pre-prepared sulfur nanoparticles (SNPs) as cores. The resulting S@CoNiMOFs could effectively inhibit shuttle effect by physical selective confinement and confined adsorption, while

shorter M–S bonds promoting the nano-conversion of sulfur species. As a result, the pouch cell with S@CoNiMOF cathode provided a capacity of 3.8 mAh cm^{-2} under a sulfur loading of 4.6 mg cm^{-2}.

In addition to monometallic and bimetallic MOFs, researchers also developed trimetallic MOFs for LSBs. Li et al.[72] prepared a series of bimetallic and even trimetallic MOF-100 structures based on Mn-MIL-100 using a one-pot synthetic approach (Figure 5f). This method introduced metal ions that cannot directly form monometallic MOF into Mn-based MOF. These multimetallic Mn-based MOF nano-octahedra were employed as sulfur hosts in LSBs. Among them, the MnNi-MIL-100@S cathode showed the best electrochemical performance, maintaining about 707.8 mAh g^{-1} after 200 cycles, much higher than that of monometallic Mn-MIL-100. This is attributed to the abundant redox active sites and surface catalytic properties afforded by bimetallic MIL-100 structure. Furthermore, the strong Lewis acid-base interactions between the Ni center and polysulfide anions benefit catalytic efficiency.

4.2. Modified Catalytic MOFs

Besides those MOFs with intrinsic catalytic capabilities, the tunable structure of MOFs provides significant flexibility to modify them for obtaining or improving the nano-confined catalytic performance through various strategy. This section will discuss recent studies about catalytically modified MOFs for LSBs.

4.2.1. Modified Catalytic MOFs for Interlayer

Indium based catalysts have proven effective in accelerating the conversion of LiPSs.[84] Cheng et al.[24a] designed a multifunctional interlayer (In/Zr-BTB nanosheets) by partially exchanging metal ion with catalytic indium. The nanosheets combine the uniform pore structure like Zr-BTB with the catalytic activity of indium, effectively inhibiting the migration of LiPSs, facilitating the transport of Li^+, and catalyzing their conversion. As a result, the LSBs with In/Zr-BTB@PP separators exhibited rate capacities of 897.96 and 735.64 mAh g^{-1} at 1 C and 3 C respectively. Furthermore, the battery maintains a capacity of 679.5 mAh g^{-1} after 500 cycles from an initial capacity of 840.7 mAh g^{-1} at 2 C, with a low decay rate of 0.039%. Even at a sulfur loading of 3.3 mg cm^{-2}, it retained 85.6% of its capacity after 300 cycles at 2 C.

The strategy for constructing single-atom catalysts (SACs) is considered to maximize the atom utilization efficiency (approaching 100%) while improving catalytic properties.[85] Because of the well-defined and tailored structures, MOFs offer distinct advantages for precisely fabricating SACs. For instance, Hu et al.[86] developed zirconium-based MOF incorporating cobalt porphyrin ligands on CNT (PCN@CNT) as interlayers in LSBs. The microstructure presents a grape-like morphology composed of oval PCN nanoparticles intergrown CNT (Figure 6a). This unique network structure not only facilitates

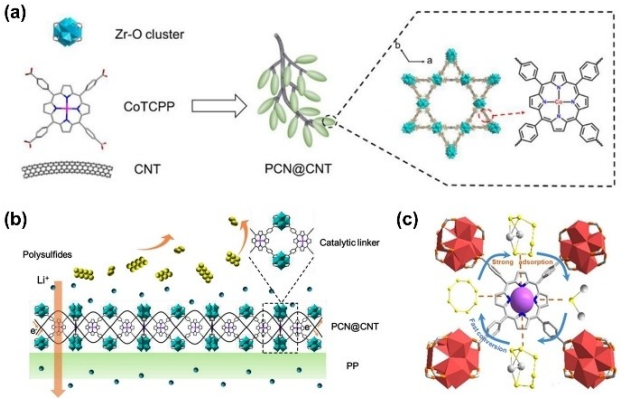

Figure 6. (a) Fabrication illustration of PCN@CNT. (b) Schematic illustrating the function of PCN@CNT for suppressing the polysulfide shuttle. Reprinted with permission.[86] Copyright 2021, Elsevier. (c) Schematic depiction of PCN-222(M)-NS. Reprinted with permission.[87] Copyright 2023, Elsevier.

electron transfer but also prevents aggregation of PCN particles, which is conducive to inhibit and capture LiPSs for potential reuse (Figure 6b). Moreover, Co and N sites in the cobalt porphyrin structure exhibit strong affinity to LiPSs and intrinsic electrocatalytic properties, promoting rapid transformation kinetics of polysulfides into Li_2S. In the reverse reaction, the conversion of solid Li_2S back into polysulfides is also accelerated. As a result, the LSBs with PCN@CNT interlayers showed a high discharge capacity (1157 mAh g^{-1} at 0.1 C) and great cycling stability (with an average degradation of 0.067% per cycle at 1 C upon 500 cycles).

To further elucidate the catalytic mechanism of metal-decorated PCN, Li et al.[87] synthesized a series of PCN-222(M) nanosheets (PCN-222(M)-NSs) possessing rational-designed M-N_4 (M=Fe^{3+}, Co^{2+}, Ni^{2+}, and Cu^{2+}) single-atom metal sites via post-synthetic modification (Figure 6c). Electrochemical experiments and DFT calculations suggest that PCN-222(Cu)-NSs exhibit the best effect in weakening S–S bond and acceleration of sulfur reduction reactions due to efficient *d-p* orbital hybridization between Cu-N_4 and LiPSs. The LSBs with PCN-222(Cu)-Ns/graphene interlayers showed a high initial capacity of 939.9 mAh g^{-1} and a low-capacity decay rate of 0.046% after 500 cycles at 1 C.

Defect engineering strategy can effectively expose more active sites which endows or promotes the nano-confined adsorption and catalysis effect of MOFs on the conversion of LiPSs.[88] The framework flexibility of MOF allows for the deliberate exposure of metal centers through rational defect design. Wu and co-workers[89] constructed a bilayer separator by coating defective HKUST on the cathode side while defect-free HKUST on the opposite side (Figure 7a). The linker-missing defects enhance the anchoring efficiency and catalytic activity of Cu sites. Meanwhile, the defect-free HKUST on the anode side facilitates rapid and uniform Li^+ transport, thereby preventing the formation of dendrites. The LSBs employing bilayer MOFs separator demonstrated stable cycling performance, with a degradation rate of 0.06% per cycle after 1000 cycles at 1 C.

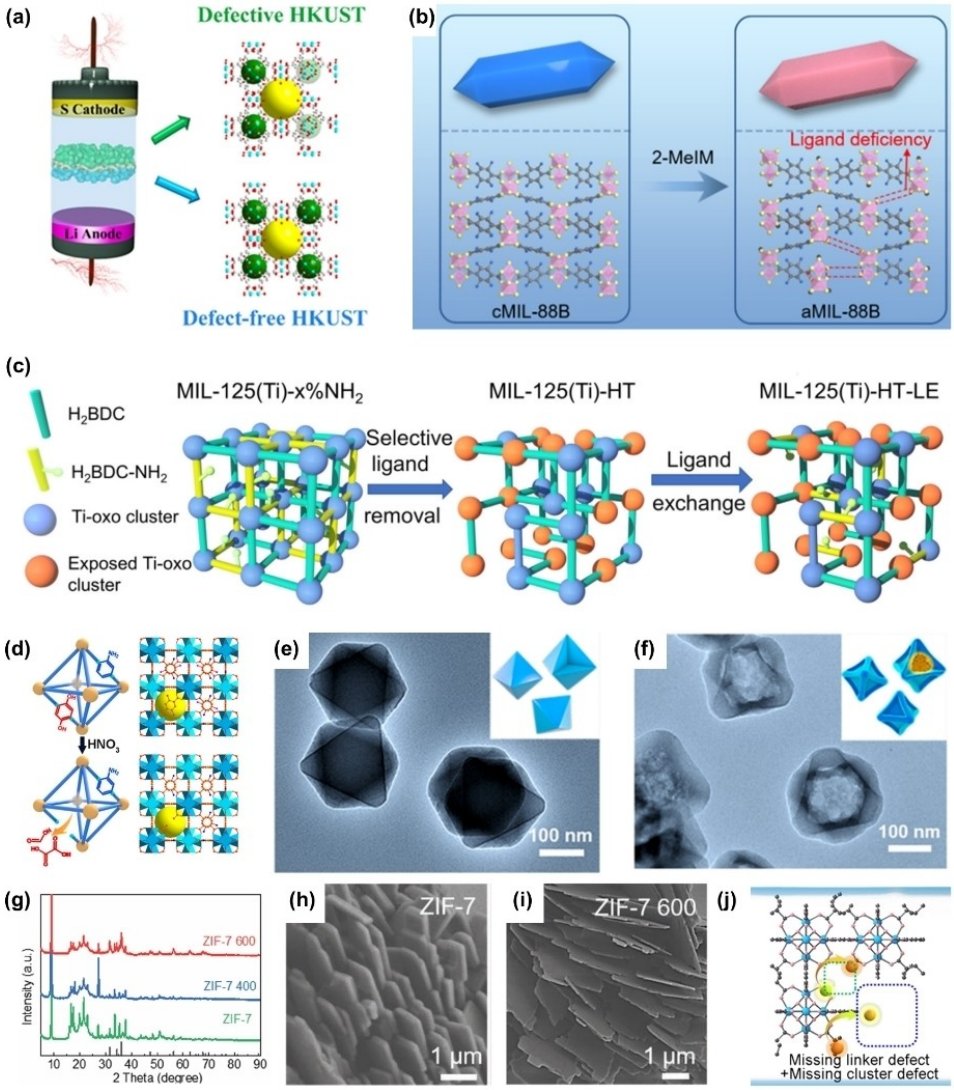

Figure 7. (a) Scheme of defective and defect-free HKUST as interlayers within the bilayer separator in LSBs. Reprinted with permission.[89] Copyright 21, Elsevier. (b) Scheme illustrating the amorphization process towards aMIL-88B. Reprinted with permission.[90] Copyright 2021, Elsevier. (c) Design strategy of Ti-MTV-MOF with catalytic centers and adsorption sites. Reprinted with permission.[26m] Copyright 2023 Elsevier. (d) Schematic diagram for D-UiO-66-NH_2. The TME images of (e) UiO-66-$(OH)_2$-NH_2-4 and (f) D-UiO-66-$(OH)_2$-NH_2-4. Reprinted with permission.[49] Copyright 2021, American Chemical Society. (g) The XRD pattern of ZIF-7, ZIF-7 400, and ZIF-7 600. The SEM images of (h) ZIF-7 and (i) ZIF-7 600. Reprinted with permission.[65] Copyright 2022, Wiley-VCH. (j) Schematic illustration of UiO-66D2. Reprinted with permission.[91] Copyright 2023, Wiley-VCH.

Amorphization induced by coordination deficiency within MOF matrix shows promise in enhancing sulfur reaction efficiency in LSBs. Zhang et al.[90] proposed a novel strategy involving amorphization of MOF via a simple ligand competition method exemplified by MIL-88B. The aMIL-88B was prepared by partial substitution of amino terephthalate in pristine cMIL-88B with 2-MeIM (Figure 7b). The chemical affinity of aMIL-88B towards LiPSs is attributed to the tendency of Li in Li_2S_6 to accept electrons and bond with O, while the terminal S prefers Fe site to form Fe–S bonds. The multi-range porous structure of aMIL-88B provides enriched ion transfer channels, and its higher surface area exposes more active sites, thereby enhancing physical and chemical interactions with LiPSs. Experimental results show that aMIL-88B exhibits a superior catalytic activity and electrochemical performance. The LSBs with the aMIL-88B modified separator realized a capacity retention of 740 mAh g^{-1} after 500 cycles at 1 C.

Guo et al.[26m] utilized ligand removal and ligand exchange (LE) to regulate a series of MOFs containing ligands with different thermal stabilities, thereby exposing catalytic metal clusters and introducing additional adsorption sites, transforming inert MOFs into catalytic ones. Specifically, selectively removal of thermally unstable ligands exposes metal clusters, which can then be substituted with adsorptive ligands (Figure 7c). The catalytic MOFs effectively trap LiPSs and simultaneously accelerate redox reduction of sulfur (RRS). The LSBs with the regulated MOF (MIL-125(Ti)-HT-LE) as the interlayer achieved excellent cyclability with a capacity decay rate of 0.024 % per cycle after 800 cycles at 1 C.

Li et al.[49] developed a defected-UiO-66-NH_2-4/graphene electrocatalytic membrane (D-UiO-66-NH_2-4/G EM) that enhances the electrochemical performance of LSBs (Figure 7d). They introduced a defect engineering strategy based on targeted nitrolysis of UiO-66$(OH)_2$-NH_2 precursors, achieving controlled framework scissoring TEM images reveal a meticulous inner structure with flocculent networks and surface pinhole formation post-treatment (Figure 7e and f). DFT calculation and analyses suggest that D-UiO-66-NH_2 can weaken the Li–S bond, reducing the decomposition barriers of Li_2S. By tuning the defect at a molecular level, D-UiO-66-NH_2 could expedite bidirection conversion of LiPSs between the intermediates and the final product of Li_2S. This electrocatalytic membrane allows LSBs to achieve an ultralong cycle life at 3 C with a capacity decay rare of 0.01 % per cycle after 600 cycles.

Wang et al.[65] designed a porous 2D defective ZIF-7 with abundant active edges under a temperature of 600 C to serve as multifunctional sulfur host materials (Figure 7g). The structure of the prepared ZIF-7 600 remained intact post-calcination (Figure 7h and i). The results show that the generation of pores exposes numerous sites, with introduced N defects forming active edges that control the electronic structure of ZIF-7. The LSBs with S/ZIF-7 600 cathode exhibited great long-term cycling performance with a low-capacity decay rate of 0.05 % per cycle for 500 cycles at 1 C. Moreover, it achieved an areal capacity of 5.2 mAh cm^{-2} under a sulfur loading of 7.6 mg cm^{-2} at 0.1 C after 50 cycles. Their group also developed a novel dual-defect MOF (missing linker and missing cluster defects) to achieve synergistic catalysis for multistep conversion reaction of LiPSs (Figure 7j).[91] The results suggest that defect-rich UiO-66 modified separator can mitigate the shuttle effect, thereby improving the LSBs performance with a capacity of 785 mAh g^{-1} after 500 cycles at 1 C. The 0.3 Ah pouch cell with the modified separator retained a capacity of 1173.9 mAh g^{-1} at 1 C after 100 cycles.

Xiao et al.[50] developed three Bi-MOFs (Bi-MOF-1, Bi-MOF-2, and Bi-MOF-3) differing in the exposure of catalytic open metal sites (Figure 8a). The porous structure of Bi-MOFs facilitates the migration of LiPSs towards inner catalytic sites rather than those on surface. Bi-MOFs can activate catalytic activity by exposing metal sites (Bi-MOF-1) or deactivate them naturally or artificially (Bi-MOF-2 and Bi-MOF-3). Among them, Bi-MOF-1 exhibits the highest surface area and a microporous structure with a window size of 7.6 Å, allowing LiPSs with a size of

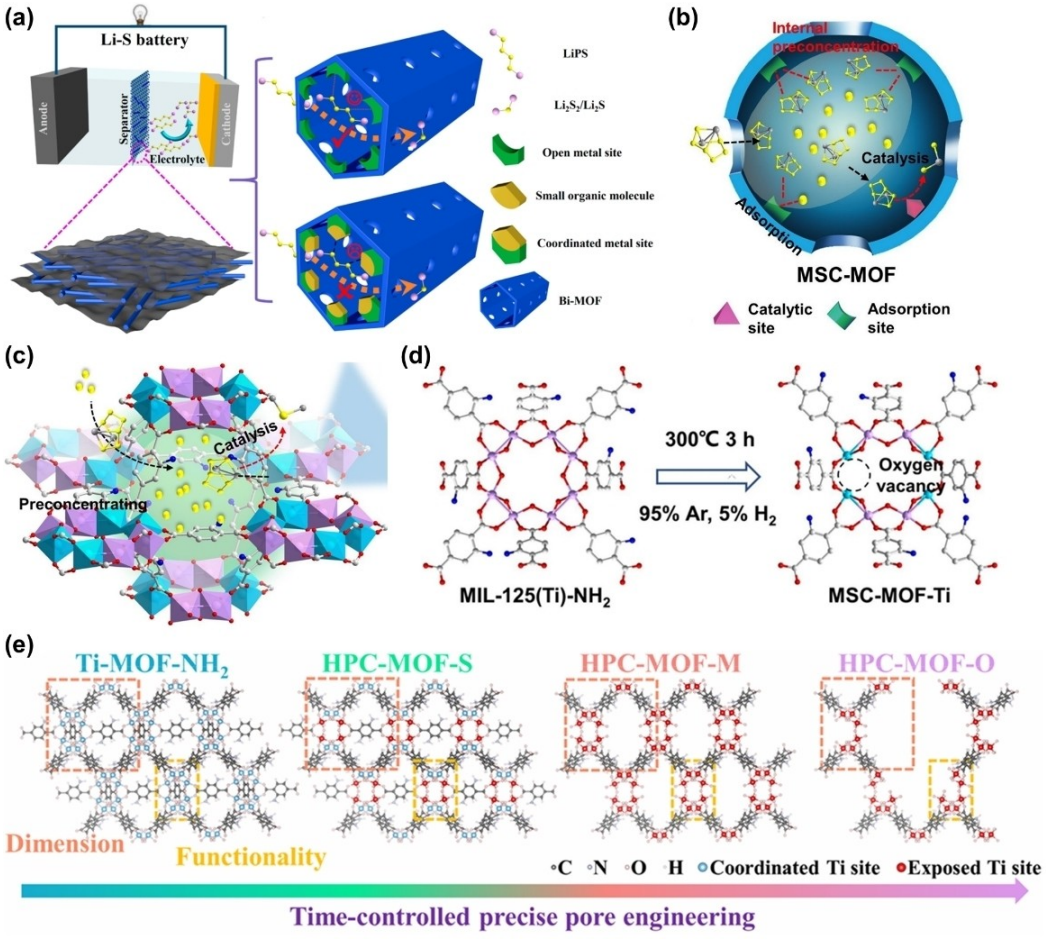

Figure 8. (a) Illustration depicting regulation of active sites in Bi-MOF-1 for LSBs. Reprinted with permission.[50] Copyright 2021, American Chemical Society. (b) Schematic illustrating the catalytic conversion processes of LiPSs. (c) Schematic illustrating the preparation of MSC-MOF-M. (d) Schematic illustration of MSC-MOF-Ti. Reprinted with permission.[26n] Copyright 2024 Wiley-VCH. (e) Time-controlled precise pore engineering for preparation of HPC-MOF-M. Reprinted with permission.[26o] Copyright 2024, American Chemical Society.

approximately 5 Å to access it. This provides a preconception for efficient nano-confined adsorption and catalysis. On this basis, Bi-MOF-1 leverages Lewis acid-base interactions between Bi^{3+} and sulfur in LiPSs, along with the catalytic capability of open metal sites. The calculation result indicates that Bi-MOF-1 can decrease the reaction barrier from Li_2S_2 to Li_2S. Moreover, Bi-MOF-1 improved the specific capacity of LSBs by 50% and reduced the decay rate by 80% after 1000 cycles at 1 C compared to those without Bi-MOF-1 as interlayers. Furthermore, pouch cells assembled with Bi-MOF-1 maintained a discharge capacity of 971.6 mAh g^{-1} after 60 cycles at 0.1 C.

To further regulate diffusion processes and enhance catalytic efficiency within MOFs, Lu et al.[26n] designed a class of multi-site catalytic MOFs (MSC-MOFs) through multimodal engineering (Figure 8b and c). After hydrogen reduction, metal sites are exposed and ionic conductivity increase due to the introduction of oxygen vacancy (Figure 8d). In addition, the $-NH_2$ groups in MOFs efficiently anchor LiPSs around catalytic metal sites via chemically-driven mass transfer, rather than relying solely on concentration diffusion. As a result, the LSBs assembled with MSC-MOF-Ti interlayer achieved a high capacity of 875.8 mAh g^{-1} at 3 C, and a high areal capacity of 11.57 mAh cm^{-2} at a high sulfur loading of 9.32 mg cm^{-2} under lean electrolyte condition. Furthermore, the pouch cell demonstrated an energy density of 350.8 Wh kg^{-1}.

To balance the mass transfer and catalytic sites, Xie et al.[26o] prepared hierarchical porous catalytic MOFs (HPC-MOFs) with tailored porosity and abundant adsorption/catalytic sites through time-controlled precise pore engineering. After etching, the pore structure of Ti-MOF-NH_2 transitions from micropores to hierarchical pores, exposing metal sites (Figure 8e). Consequently, HPC-MOFs-M facilitate rapid reactant transfer through large pore, while maintaining a high density of catalytic sites in existing micropores, thereby enhancing catalytic efficiency. As a result, the LSBs with HPC- MOFs-M interlayer obtained a low decay rate of 0.053% per cycle over 500 cycles at 1 C.

4.2.2. Modified Catalytic MOFs for Host

The classic ZIF-8 MOF from the ZIF series is widely used to physically block the diffusion of LiPSs, but its catalytic properties are rarely discussed, making suppression of the shuttle effect challenging due to LiPSs accumulation from slow redox reaction.[37,55,92] To develop the catalysis of ZIF-8, Cui et al.[60] synthesized a 3D ordered macro-microporous MOF (3DOM-MOF) via a self-templated coordination-replication method. The resulting 3DOM ZIF-8 features ordered macro- and micropore synergistically, facilitating electrolyte infiltration, charge transport, and offering a high surface area with rich Zn sites for adsorption and catalysis. Consequently, the LSBs assembled with the cathodes based on 3DOM ZIF-8 displayed excellent cycling stability over 500 cycles with a low-capacity fading rate of 0.028% per cycle, and a high capacity of 803 mAh g^{-1} at 2 C.

He et al.[67] proposed a universal MOF-confined strategy to synthesize atomically dispersed metal catalysts (ADMCs) using ethylenediaminetetraacetic acid (EDTA) as coupling agent for chemical bonding with unsaturated sites and chelating agent to anchor metal sites (Figure 9a). The atomically dispersed M-N_2O_2 sites in prepared MOF-808-M (M = different metal) enhance the chemical interaction with LiPSs and promote reaction kinetics by reducing the energy barrier of the rate-limiting step.

In another work, Zhu and co-workers[69] design a conductive bimetallic MOF nanoboxes (ZnCo-MOF NBs) with atomically dispersed Co-O_4 sites via cation and ligand exchange. The Co-O_4 sites in MOFs structure exhibit strong adsorption capabilities for LiPSs and accelerate their conversion kinetics. Meanwhile, the hollow structure allows for high sulfur loading and accommodates volume expansion during cycling.

Researchers have found the significant potential of incorporating catalytically active species into MOFs pores, particularly in the realms of energy storage and electrocatalysis.[93] Recently, Zeng and co-workers[26l] integrated sub-nanometer Ti—O clusters (TOCs) into the MOFs pores, designing a highly efficient catalytic sulfur host for LSBs named as MOF-TOC (Figure 9b). They utilized MIL-101(Cr) as the precursor due to its large pores, which are more conducive to sulfur storage and ion diffusion facilitation. The sub-nanometer catalysts formed within the MOF pores while maintaining the original structure. The Ti and O components of TOCs interact independently with S and Li in LiPSs, indicating the excellent nano-confined adsorption capabilities for LiPSs of MOF-TOC. Furthermore, the internal TOCs accelerate the reaction kinetics of LiPSs via d-p orbital hybridization between Ti and S. In contrast to TiO@MOF configurations with larger size TiO_2 particles on MOF surface, MOF-TOC with sub-nano TOCs in pores provides more active sites, enhancing sulfur adsorption capacity and catalytic conversion efficiency. At a high sulfur loading of 8.0 mg cm^{-2}, LSBs using MOFs-TOC as the sulfur host exhibited a significant areal capacity of 7.9 mAh cm^{-2} at 0.1 C, which exhibited minimal degradation after 50 cycles.

The configuration match and electric structure are also vital for promote the conversion of LiPSs. Building on their previous work, Xiao et al. elaborated a series of dual-active-center MOFs (D-MOFs).[68] The aim was to match the configuration of long-chain LiPSs and optimized the metal-sulfur orbital hybridization by regulating the distance between different polar active sites and the electronic structure of the metal center (Figure 9c). The dual catalytic centers in D-MOFs exhibited a higher configuration compatibility for various LiPSs as evidenced by simulated calculations and electrochemical experiments. Furthermore, the mediated metal catalytic site in M-N_4 (M=Co, Ni, Cu) optimized the electronic structures and efficient metal-sulfur hybridization. According to the Sabatier principle, moderate adsorption is critical for catalytic efficiency. Combining these factors, D-MOF-Cu achieved the superior battery performance as a sulfur host material, attributed to its moderate interaction with LiPSs and optimal catalytic sites. By in situ assembly of D-MOFs on CNTs, an efficient host was achieved with excellent long cycling stability, high areal capacity (10.04 mAh cm^{-2} at a high loading of 14.3 mg cm^{-2}), and a stable working of a pouch cell delivering 310.7 Wh kg^{-1}.

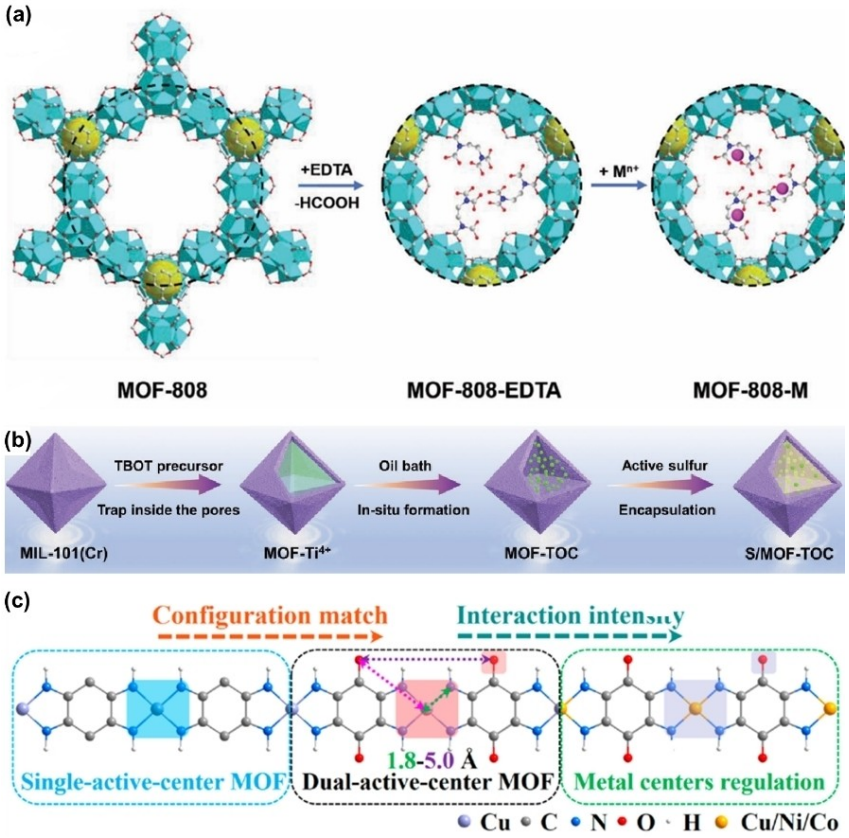

Figure 9. (a) Schematic illustrating the preparation for MOF-808-M. Reprinted with permission.[67] Copyright 2023, Wiley-VCH. (b) Schematic illustrating the preparation process of MOF-TOCs. Reprinted with permission.[26l] Copyright 2023 Wiley-VCH. (c) Regulation of interaction intensity via mediating the electronic structure of metal centers. Reprinted with permission.[68] Copyright 2023, American Chemical Society.

5. Conclusion and Outlook

LSBs represent one of the most potential next-generation energy storage devices due to their high theoretical energy density, elevated specific capacity of sulfur cathode. However, the shuttle effect and sluggish redox kinetics of LiPSs significantly impact their electrochemical performance. MOFs have emerged as multifunctional candidates for addressing these issues in LSBs, owing to their high porosity, uniform pore size distribution, customizable structures, and ease of functionalization. These attributes make MOFs well-suited for various roles within LSBs, including serving as sulfur hosts, interlayers, and even separators. This review systematically summarizes the nano-confinement effects of MOFs for LSBs. The advantages of MOFs for LSBs were first highlighted. Then detailed discussions on the specific application of MOFs in LSBs were held, including selective confinement and nano-confined adsorption by inert MOFs, as well as nano-confined catalysis facilitated by catalytically active MOFs.

The requirements for MOFs in LSBs are increasing stringent. For the design and utilization of MOFs in LSBs, there are some basic rules should be followed. Firstly, the porous structure of MOFs should be strategically designed to facilitate mass transfer and sulfur loading. MOFs can also mitigate polysulfide diffusion by regulating pore size and incorporating negative charged groups when used as interlayer or separator. Additionally, MOFs must exhibit sufficient adsorption capability for LiPSs to mitigate their diffusion, which can be achieved by functionalizing ligands to improve chemical interactions between MOFs and LiPSs. Furthermore, to address the sluggish redox kinetics and reduce the shuttle effect caused by accumulation of LiPSs, MOFs should be engineered with catalytic activity. This can be accomplished through metal cluster engineering and catalyst doping, which accelerate the conversion of LiPSs (Figure 10).

Despite their considerable potential, the application of MOFs in LSBs is still nascent, beset by numerous challenges that need to be addressed.

(1) The application of MOFs in LSBs faces several obstacles, including high costs and complex preparation processes. Transition metals such as cobalt and zirconium are commonly employed as catalytic elements in MOFs due to their excellent activity. However, their scarcity and uneven global distribution contribute to elevated cost. Exploring alternative MOFs containing low-cost metals like cerium can effectively mitigate this issue. Additionally, the complex synthetic processes involved in MOFs production, typically utilizing organic solvents or high temperatures, increase both costs and difficulty of production. Fortunately, recent research has shown the feasibility of preparing MOFs using water as a solvent or employing ultrasonic or mechano-

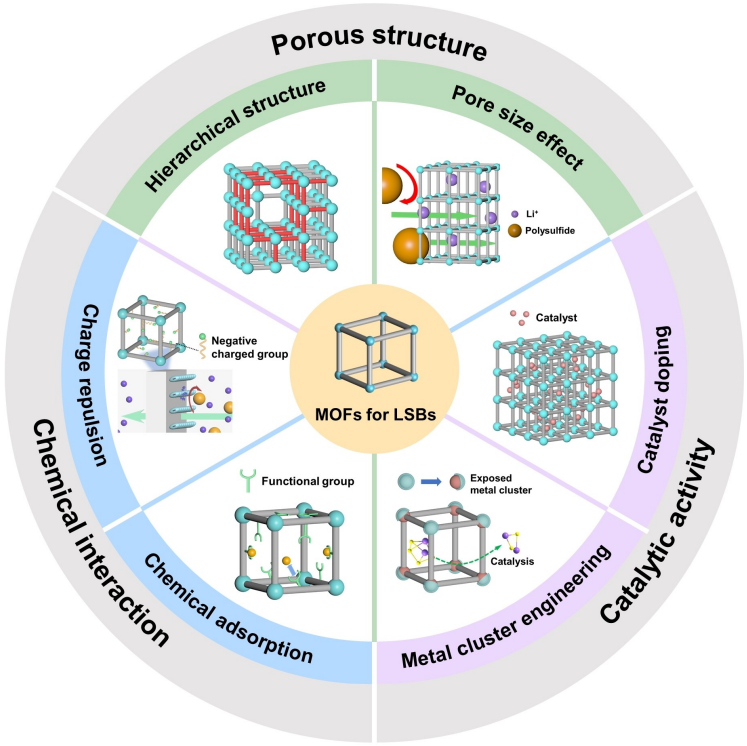

Figure 10. The rules of design and utilization of MOFs for LSBs.

chemical methods, simplifying the fabrication processes and potentially reducing costs. These advancements promise to overcome barriers to widespread implementation of MOFs in LSBs.

(2) The actual energy density of LSBs significantly lags behind theoretical expectations, posing a major obstacle to their practical application. This issue is further exacerbated when MOFs are used as interlayers, increasing the weight of the batteries and impeding the achievement of high energy density. To fully exploit the potential benefits of MOFs, researchers should prioritize developing ultralight and ultrathin interlayers, or explore methods to suppress the shuttle effect at the cathode without requiring interlayers. Recent studies have introduced self-supporting MOF membranes that can directly replace commercial separators like PP, effectively inhibiting the shuttle of LiPSs. Therefore, research into MOF-based separators is crucial to addressing these challenges and optimizing LSB performance.

(3) The low conductivity of MOFs presents a significant hurdle in their use as sulfur host materials in LSBs. This low conductivity leads to severe polarization and impedes fast reaction kinetics, thereby limiting battery performance. To deal with the problem, some researchers have introduced more conductive additives or combined MOFs with conductive material, resulting in an increase in battery weight and a decrease in sulfur content, thereby compromising energy density. Developing novel conductive MOFs via strategies such as electronic structure regulation offer a promising approach to improving electrochemical performance.

(4) Although possessing a high specific surface area, the catalytic potential of MOFs is often constrained by insufficient exposure of active sites. This limitation typically arises because metal canters are fully coordinated with organic ligands in a complete MOF structure or isolated within the framework, resulting in limited available sites. To overcome this, effective approaches to increase accessibility to these sites—such as defect engineering or other innovative measures—must be explored.

(5) Despite the inherent framework flexibility of MOFs, the development of MOF-based catalysts in LSBs has predominantly followed conventional catalysts mechanisms. Leveraging the diversity of structures and compositions achievable with MOFs could open entirely new avenues for catalysis research and development. Therefore, researchers have substantial potential to explore and harness the unique designability of MOFs in developing catalytic mechanisms.

In summary, MOFs have positioned LSBs as one of the most promising candidates for next-generation high-performance energy storage devices. Through strategic design of their flexible frameworks, the synergistic effects among structure, conductivity, metal centers and organic ligands can be precisely optimized to develop more efficient catalysts. With the emergence of groundbreaking researches, the fundamental mechanisms underlying MOFs are gradually being understood, paving the way for the ongoing advancements in LSBs and other energy storage devices.

Acknowledgements

The authors gratefully acknowledge financial support from the National Natural Science Foundation of China(No. 51920105004, 52090021), the Natural Science Foundation of Guangzhou, China(2023 A04 J1602) and the Open Project Program of State Key Laboratory of Silicon and Advanced Semiconductor Materials(SKL2023-11).

Conflict of Interests

The authors declare no conflict of interest.

Keywords: Metal-organic frameworks · Lithium-sulfur batteries · Nano-confinement effect · Catalysis · Energy conversion

[1] a) Z. Xing, G. Tan, Y. Yuan, B. Wang, L. Ma, J. Xie, Z. Li, T. Wu, Y. Ren, R. Shahbazian-Yassar, *Adv. Mater.* **2020**, *32*, 2002403; b) X. Liu, Q. He, H. Yuan, C. Yan, Y. Zhao, X. Xu, J.-Q. Huang, Y.-L. Chueh, Q. Zhang, L. Mai, *J. Energy Chem.* **2020**, *48*, 109; c) B. Zhang, C. Luo, Y. Deng, Z. Huang, G. Zhou, W. Lv, Y. B. He, Y. Wan, F. Kang, Q. H. Yang, *Adv. Energy Mater.* **2020**, *10*, 2000091; d) Y.-X. Song, Y. Shi, J. Wan, S.-Y. Lang, X.-C. Hu, H.-J. Yan, B. Liu, Y.-G. Guo, R. Wen, L.-J. Wan, *Energy Environ. Sci.* **2019**, *12*, 2496; e) W.-J. Chen, C.-X. Zhao, B.-Q. Li, Q. Jin, X.-Q. Zhang, T.-Q. Yuan, X. Zhang, Z. Jin, S. Kaskel, Q. Zhang, *Energy Environ. Mater.* **2020**, *3*, 160; f) W. P. Wang, J. Zhang, J. Chou, Y. X. Yin, Y. You, S. Xin, Y. G. Guo, *Adv. Energy Mater.* **2020**, *11*, 2000791.

[2] a) X. Chen, Z. Xiao, X. Ning, Z. Liu, Z. Yang, C. Zou, S. Wang, X. Chen, Y. Chen, S. Huang, *Adv. Energy Mater.* **2014**, *4*, 1301988; b) T. Wang, Q. Zhang, J. Zhong, M. Chen, H. Deng, J. Cao, L. Wang, L. Peng, J. Zhu, B. Lu, *Adv. Energy Mater.* **2021**, *11*, 2100448.

[3] Z. Zhao, S. Wang, R. Liang, Z. Li, Z. Shi, G. Chen, *J. Mater. Chem. A* **2014**, *2*, 13509.

[4] a) Y. Xiao, S. Guo, Y. Ouyang, D. Li, X. Li, W. He, H. Deng, W. Gong, C. Tan, Q. Zeng, Q. Zhang, S. Huang, *ACS Nano* **2021**, *15*, 18363; b) J. He, Y. Chen, W. Lv, K. Wen, C. Xu, W. Zhang, Y. Li, W. Qin, W. He, *ACS Nano* **2016**, *10*, 10981; c) X. Tao, J. Wang, C. Liu, H. Wang, H. Yao, G. Zheng, Z. W. Seh, Q. Cai, W. Li, G. Zhou, C. Zu, Y. Cui, *Nat. Commun.* **2016**, *7*, 11203.

[5] a) W. Hua, H. Li, C. Pei, J. Xia, Y. Sun, C. Zhang, W. Lv, Y. Tao, Y. Jiao, B. Zhang, S. Z. Qiao, Y. Wan, Q. H. Yang, *Adv. Mater.* **2021**, *33*, 2101006; b) S. Zhai, Z. Ye, R. Liu, H. Xu, C. Li, W. Liu, X. Wang, T. Mei, *Adv. Funct. Mater.* **2023**, *34*, 2314379.

[6] a) C. Yuan, X. Yang, P. Zeng, J. Mao, K. Dai, L. Zhang, X. Sun, *Nano Energy* **2021**, *84*, 105928; b) Z. Yuan, H. J. Peng, T. Z. Hou, J. Q. Huang, C. M. Chen, D. W. Wang, X. B. Cheng, F. Wei, Q. Zhang, *Nano Lett.* **2016**, *16*, 519.

[7] a) J. Xu, W. Tang, C. Yang, I. Manke, N. Chen, F. Lai, T. Xu, S. An, H. Liu, Z. Zhang, Y. Cao, N. Wang, S. Zhao, D. Niu, R. Chen, *ACS Energy Lett.* **2021**, *6*, 3053; b) C. Ma, Y. Zhang, Y. Feng, N. Wang, L. Zhou, C. Liang, L. Chen, Y. Lai, X. Ji, C. Yan, W. Wei, *Adv. Mater.* **2021**, *33*, 2100171; c) L. Wang, W. Hua, X. Wan, Z. Feng, Z. Hu, H. Li, J. Niu, L. Wang, A. Wang, J. Liu, X. Lang, G. Wang, W. Li, Q. H. Yang, W. Wang, *Adv. Mater.* **2022**, *34*, 2110279.

[8] a) M. Li, Y. Wang, S. Sun, Y. Yang, G. Gu, Z. Zhang, *Chem. Eng. J.* **2022**, *429*, 132254; b) Y. Liang, T. Xia, Z. Chang, W. Xie, Y. Li, C. Li, R. Fan, W. Wang, Z. Sui, Q. Chen, *Chem. Eng. J.* **2022**, *437*, 135314; c) J. K. Huang, M. Li, Y. Wan, S. Dey, M. Ostwal, D. Zhang, C. W. Yang, C. J. Su, U. S. Jeng, J. Ming, A. Amassian, Z. Lai, Y. Han, S. Li, L. J. Li, *ACS Nano* **2018**, *12*, 836; d) Y. He, Z. Chang, S. Wu, Y. Qiao, S. Bai, K. Jiang, P. He, H. Zhou, *Adv. Energy Mater.* **2018**, *8*, 1802130; e) G. Gao, Y. Wang, S. Wang, R. X. Yang, Y. Chen, Y. Zhang, C. Jiang, M. J. Wei, H. Ma, Y. Q. Lan, *Angew. Chem. Int. Ed.* **2021**, *60*, 10147; f) L. Fan, S. Chen, J. Zhu, R. Ma, S. Li, R. Podila, A. M. Rao, G. Yang, C. Wang, Q. Liu, Z. Xu, L. Yuan, Y. Huang, B. Lu, *Adv. Sci.* **2018**, *5*, 1700934.

[9] a) X. Ji, K. T. Lee, L. F. Nazar, *Nat. Mater.* **2009**, *8*, 500; b) G. He, X. Ji, L. Nazar, *Energy Environ. Sci.* **2011**, *4*, 2878; c) D.-W. Wang, Q. Zeng, G. Zhou, L. Yin, F. Li, H.-M. Cheng, I. R. Gentle, G. Q. M. Lu, *J. Mater. Chem. A* **2013**, *1*, 9382.

[10] a) B. Ding, C. Yuan, L. Shen, G. Xu, P. Nie, Q. Lai, X. Zhang, *J. Mater. Chem. A* **2013**, *1*, 1096; b) M. Yu, R. Li, M. Wu, G. Shi, *Energy Storage Mater.* **2015**, *1*, 51; c) J. Zhang, J.-Y. Li, W.-P. Wang, X.-H. Zhang, X.-H. Tan, W.-G. Chu, Y.-G. Guo, *Adv. Energy Mater.* **2018**, *8*, 1702839.

[11] a) A. Abdul Razzaq, Y. Yao, R. Shah, P. Qi, L. Miao, M. Chen, X. Zhao, Y. Peng, Z. Deng, *Energy Storage Mater.* **2019**, *16*, 194; b) X.-B. Cheng, J.-Q. Huang, Q. Zhang, H.-J. Peng, M.-Q. Zhao, F. Wei, *Nano Energy* **2014**, *4*, 65.

[12] J. Zhang, C. P. Yang, Y. X. Yin, L. J. Wan, Y. G. Guo, *Adv. Mater.* **2016**, *28*, 9539.

[13] a) P. Wang, B. Xi, M. Huang, W. Chen, J. Feng, S. Xiong, *Adv. Energy Mater.* **2021**, *11*, 2002893; b) S. F. Ng, M. Y. L. Lau, W. J. Ong, *Adv. Mater.* **2021**, *33*, 2008654; c) P. Chen, T. Wang, D. He, T. Shi, M. Chen, K. Fang, H. Lin, J. Wang, C. Wang, H. Pang, *Angew. Chem. Int. Ed.* **2023**, *62*, e202311693.

[14] a) A. Henrique, T. Maity, H. Zhao, P. F. Brântuas, A. E. Rodrigues, F. Nouar, A. Ghoufi, G. Maurin, J. A. C. Silva, C. Serre, *J. Mater. Chem. A* **2020**, *8*, 17780; b) D. Feng, Z. Gu, J. Li, H. L. Jiang, Z. Wei, H. C. Zhou, *Angew. Chem. Int. Ed.* **2012**, *124*, 10453; c) L. Jiao, J. Y. R. Seow, W. S. Skinner, Z. U. Wang, H.-L. Jiang, *Mater. Today* **2019**, *27*, 43.

[15] a) M. F. Ghazvini, M. Vahedi, S. N. Nobar, F. Sabouri, *J. Environ. Chem. Eng.* **2021**, *9*, 104790; b) I. Abánades Lázaro, C. J. R. Wells, R. S. Forgan, *Angew. Chem. Int. Ed.* **2020**, *132*, 5249; c) Y. B. N. Tran, P. T. K. Nguyen, Q. T. Luong, K. D. Nguyen, *Inorg. Chem.* **2020**, *59*, 16747; d) Z. Ye, Y. Jiang, L. Li, F. Wu, R. Chen, *Nano-Micro Lett.* **2021**, *13*, 203; e) Y. Ouyang, W. Gong, Q. Zhang, J. Wang, S. Guo, Y. Xiao, D. Li, C. Wang, X. Sun, C. Wang, S. Huang, *Adv. Mater.* **2023**, *35*, 2304685; f) Y. Cui, B. Li, H. He, W. Zhou, B. Chen, G. Qian, *Acc. Chem. Res.* **2016**, *49*, 483; g) G. Yuan, L. Tan, P. Wang, Y. Wang, C. Wang, H. Yan, Y.-Y. Wang, *Cryst. Growth Des.* **2021**, *22*, 893.

[16] a) X. Liu, S. Wang, A. Wang, Z. Wang, J. Chen, Q. Zeng, P. Chen, W. Liu, Z. Li, L. Zhang, *J. Mater. Chem. A* **2019**, *7*, 24515; b) A. E. Baumann, X. Han, M. M. Butala, V. S. Thoi, *J. Am. Chem. Soc.* **2019**, *141*, 17891.

[17] J. Zhou, R. Li, X. Fan, Y. Chen, R. Han, W. Li, J. Zheng, B. Wang, X. Li, *Energy Environ. Sci.* **2014**, *7*, 2715.

[18] S. Y. Bai, X. Z. Liu, K. Zhu, S. C. Wu, H. S. Zhou, *Nat. Energy* **2016**, *1*, 16094.

[19] M. Li, Y. Wan, J.-K. Huang, A. H. Assen, C.-E. Hsiung, H. Jiang, Y. Han, M. Eddaoudi, Z. Lai, J. Ming, L.-J. Li, *ACS Energy Lett.* **2017**, *2*, 2362.

[20] J. Wang, J. Li, *J. Colloid Interface Sci.* **2021**, *584*, 354.

[21] P. Geng, M. Du, X. Guo, H. Pang, Z. Tian, P. Braunstein, Q. Xu, *Energy Environ. Mater.* **2021**, *5*, 599.

[22] a) Z. Wu, L. Wang, S. Chen, X. Zhu, Q. Deng, J. Wang, Z. Zeng, S. Deng, *Chem. Eng. J.* **2021**, *404*, 126579; b) H.-G. Jin, M. Wang, J.-X. Wen, S.-H. Han, X.-J. Hong, Y.-P. Cai, G. Li, J. Fan, Z.-S. Chao, *ACS Appl. Mater. Inter.* **2021**, *13*, 3899.

[23] H. He, Y. Cui, B. Li, B. Wang, C. Jin, J. Yu, L. Yao, Y. Yang, B. Chen, G. Qian, *Adv. Mater.* **2019**, *31*, 1806897.

[24] a) Z. Cheng, J. Lian, Y. Chen, Y. Tang, Y. Huang, J. Zhang, S. Xiang, Z. Zhang, *CCS Chem.* **2023**, *6*, 988; b) G. Lu, S. Li, Z. Guo, O. K. Farha, B. G. Hauser, X. Qi, Y. Wang, X. Wang, S. Han, X. Liu, *Nat. Chem.* **2012**, *4*, 310; c) L. Bromberg, Y. Diao, H. Wu, S. A. Speakman, T. A. Hatton, *Chem. Mater.* **2012**, *24*, 1664; d) H. Fei, J. Shin, Y. S. Meng, M. Adelhardt, J. R. Sutter, K. Meyer, S. M. Cohen, *J. Am. Chem. Soc.* **2014**, *136*, 4965.

[25] X. Hu, T. Huang, G. Zhang, S. Lin, R. Chen, L.-H. Chung, J. He, *Coord. Chem. Rev.* **2023**, *475*, 214879.

[26] a) R. Demir Cakan, M. Morcrette, F. Nouar, C. Davoisne, T. Devic, D. Gonbeau, R. Dominko, C. Serre, G. Ferey, J. M. Tarascon, *J. Am. Chem. Soc.* **2011**, *133*, 16154; b) Z. Wang, X. Li, Y. Cui, Y. Yang, H. Pan, Z. Wang, C. Wu, B. Chen, G. Qian, *Cryst. Growth Des.* **2013**, *13*, 5116; c) J. Zheng, J. Tian, D. Wu, M. Gu, W. Xu, C. Wang, F. Gao, M. H. Engelhard, J. G. Zhang, J. Liu, J. Xiao, *Nano Lett.* **2014**, *14*, 2345; d) Z. Wang, B. Wang, Y. Yang, Y. Cui, Z. Wang, B. Chen, G. Qian, *ACS Appl. Mater. Inter.* **2015**, *7*, 20999; e) Y. Zang, F. Pei, J. Huang, Z. Fu, G. Xu, X. Fang, *Adv. Energy Mater.* **2018**, *8*, 1802052; f) X. Hong, C. Song, Y. Yang, H. C. Tan, G. H. Li, Y. P. Cai, H. Wang, *ACS Nano* **2019**, *13*, 1923; g) P. Chiochan, X. Yu, M. Sawangphruk, A. Manthiram, *Adv. Energy Mater.* **2020**, *10*, 2001285; h) S. Guo, Y. Xiao, J. Wang, Y. Ouyang, X. Li, H. Deng, W. He, Q. Zeng, W. Zhang, Q. Zhang, S. Huang, *Nano Res.* **2021**, *14*, 4556; i) Y. Wang, Z. Deng, J. Huang, H. Li, Z. Li, X. Peng, Y. Tian, J. Lu, H. Tang, L. Chen, Z. Ye, *Energy Storage Mater.* **2021**, *36*, 466; j) Q. Zeng, X. Li, W. Gong, S. Guo, Y.

Ouyang, D. Li, Y. Xiao, C. Tan, L. Xie, H. Lu, Q. Zhang, S. Huang, *Adv. Energy Mater.* **2022**, *12*, 2104074; k) Y. Xiao, Y. Xiang, S. Guo, J. Wang, Y. Ouyang, D. Li, Q. Zeng, W. Gong, L. Gan, Q. Zhang, S. Huang, *Energy Storage Mater.* **2022**, *51*, 882; l) Q. Zeng, L. Xu, G. Li, Q. Zhang, S. Guo, H. Lu, L. Xie, J. Yang, J. Weng, C. Zheng, S. Huang, *Adv. Funct. Mater.* **2023**, *33*, 2304619; m) S. Guo, Y. Xiao, A. Cherevan, D. Eder, L. Xu, Q. Zeng, Y. Ouyang, Q. Zhang, S. Huang, *Mater. Today* **2023**, *65*, 37; n) H. Lu, Q. Zeng, L. Xu, Y. Xiao, L. Xie, J. Yang, J. Rong, J. Weng, C. Zheng, Q. Zhang, S. Huang, *Angew. Chem. Int. Ed.* **2024**, *63*, e202318859; o) L. Xie, Y. Xiao, Q. Zeng, Y. Wang, J. Weng, H. Lu, J. Rong, J. Yang, C. Zheng, Q. Zhang, S. Huang, *ACS Nano* **2024**, *18*, 12820.

[27] a) M. Du, Q. Li, G. Zhang, F. Wang, H. Pang, *Energy Environ. Mater.* **2021**, *5*, 215; b) Z. Chu, X. Gao, C. Wang, T. Wang, G. Wang, *J. Mater. Chem. A* **2021**, *9*, 7301; c) F. Qi, Z. Sun, X. Fan, Z. Wang, Y. Shi, G. Hu, F. Li, *Adv. Energy Mater.* **2021**, *11*, 2100387.

[28] Y. Zheng, S. Zheng, H. Xue, H. Pang, *J. Mater. Chem. A* **2019**, *7*, 3469.

[29] Y. Gu, Y. N. Wu, L. Li, W. Chen, F. Li, S. Kitagawa, *Angew. Chem. Int. Ed.* **2017**, *56*, 15658.

[30] X. Ren, Q. Wang, Y. Pu, Q. Sun, W. Sun, L. Lu, *Adv. Mater.* **2023**, *35*, 2304120.

[31] S. Bai, K. Zhu, S. Wu, Y. Wang, J. Yi, M. Ishida, H. Zhou, *J. Mater. Chem. A* **2016**, *4*, 16812.

[32] Z. Chang, Y. Qiao, J. Wang, H. Deng, P. He, H. Zhou, *Energy Storage Mater.* **2020**, *25*, 164.

[33] M. Tian, F. Pei, M. Yao, Z. Fu, L. Lin, G. Wu, G. Xu, H. Kitagawa, X. Fang, *Energy Storage Mater.* **2019**, *21*, 14.

[34] Z. Wang, W. Huang, J. Hua, Y. Wang, H. Yi, W. Zhao, Q. Zhao, H. Jia, B. Fei, F. Pan, *Small Methods* **2020**, *4*, 2000082.

[35] S. Lin, J. Dong, R. Chen, G. Zhang, T. Huang, J. Li, H. Zhou, L.-H. Chung, X. Hu, J. He, *J. Alloys Compd.* **2023**, *965*, 171389.

[36] D.-D. Han, Z.-Y. Wang, G.-L. Pan, X.-P. Gao, *ACS Appl. Mater. Inter.* **2019**, *11*, 18427.

[37] F. Wu, S. Zhao, L. Chen, Y. Lu, Y. Su, Y. Jia, L. Bao, J. Wang, S. Chen, R. Chen, *Energy Storage Mater.* **2018**, *14*, 383.

[38] Y. Guo, M. Sun, H. Liang, W. Ying, X. Zeng, Y. Ying, S. Zhou, C. Liang, Z. Lin, X. Peng, *ACS Appl. Mater. Int.* **2018**, *10*, 30451.

[39] D. H. Lee, J. H. Ahn, M.-S. Park, A. Eftekhari, D.-W. Kim, *Electrochim. Acta* **2018**, *283*, 1291.

[40] C. Qi, L. Xu, J. Wang, H. Li, C. Zhao, L. Wang, T. Liu, *ACS Sustain. Chem. Eng.* **2020**, *8*, 12968.

[41] Y. Li, S. Lin, D. Wang, T. Gao, J. Song, P. Zhou, Z. Xu, Z. Yang, N. Xiao, S. Guo, *Adv. Mater.* **2020**, *32*, 1906722.

[42] J. Li, C. Jiao, J. Zhu, L. Zhong, T. Kang, S. Aslam, J. Wang, S. Zhao, Y. Qiu, *J. Energy Chem.* **2021**, *57*, 469.

[43] P. Geng, L. Wang, M. Du, Y. Bai, W. Li, Y. Liu, S. Chen, P. Braunstein, Q. Xu, H. Pang, *Adv. Mater.* **2022**, *34*, 2107836.

[44] J. H. Park, K. M. Choi, D. K. Lee, B. C. Moon, S. R. Shin, M.-K. Song, J. K. Kang, *Sci. Rep.* **2016**, *6*, 25555.

[45] P. Li, L. Ma, T. Wu, H. Ye, J. Zhou, F. Zhao, N. Han, Y. Wang, Y. Wu, Y. Li, J. Lu, *Adv. Energy Mater.* **2018**, *8*, 1800624.

[46] X. Zhang, K. Chen, Z. Sun, G. Hu, R. Xiao, H.-M. Cheng, F. Li, *Energy Environ. Sci.* **2020**, *13*, 1076.

[47] H. Kim, J. Lee, H. Ahn, O. Kim, M. J. Park, *Nat. Commun.* **2015**, *6*, 7278.

[48] a) H. Yang, J. Chen, J. Yang, J. Wang, *Angew. Chem. Int. Ed.* **2020**, *59*, 7306; b) N. Xu, T. Qian, X. Liu, J. Liu, Y. Chen, C. Yan, *Nano Lett.* **2017**, *17*, 538.

[49] S. Li, J. Lin, Y. Ding, P. Xu, X. Guo, W. Xiong, D. Y. Wu, Q. Dong, J. Chen, L. Zhang, *ACS Nano* **2021**, *15*, 13803.

[50] Y. Xiao, W. Gong, S. Guo, Y. Ouyang, D. Li, X. Li, Q. Zeng, W. He, H. Deng, C. Tan, Q. Zhang, S. Huang, *ACS Mater. Lett.* **2021**, *3*, 1684.

[51] F. Zhang, T. Niu, F. Wu, L. Wu, G. Wang, J. Li, *Electrochim. Acta* **2021**, *392*, 139028.

[52] Z. Li, Y. Sun, X. Wu, H. Yuan, Y. Yu, Y. Tan, *ACS Energy Lett.* **2022**, *7*, 4190.

[53] B. Dang, Q. Li, Y. Luo, R. Zhao, J. Li, F. Wu, *J. Alloys Compd.* **2022**, *915*, 165375.

[54] Y. Ren, Q. Zhai, B. Wang, L. Hu, Y. Ma, Y. Dai, S. Tang, X. Meng, *Chem. Eng. J.* **2022**, *439*, 135535.

[55] C. Zhou, M. Chen, C. Dong, H. Wang, C. Shen, X. Wu, Q. An, G. Chang, X. Xu, L. Mai, *Nano Energy* **2022**, *98*, 107332.

[56] T. Guo, Y. Ding, C. Xu, W. Bai, S. Pan, M. Liu, M. Bi, J. Sun, X. Ouyang, X. Wang, Y. Fu, J. Zhu, *Adv. Sci.* **2023**, *10*, 2302518.

[57] L. Li, Y. Luo, Y. Wang, Z. Zhang, F. Wu, J. Li, *Chem. Eng. J.* **2023**, *454*, 140043.

[58] L. Li, H. Tu, J. Wang, M. Wang, W. Li, X. Li, F. Ye, Q. Guan, F. Zhu, Y. Zhang, Y. Hu, C. Yan, H. Lin, M. Liu, *Adv. Funct. Mater.* **2023**, *33*, 2212499.

[59] Y. Yang, S. Ma, M. Xia, Y. Guo, Y. Zhang, L. Liu, C. Zhou, G. Chen, X. Wang, Q. Wu, L. Yang, Z. Hu, *Mater. Today Phys.* **2023**, *35*, 101112.

[60] G. Cui, G. Li, D. Luo, Y. Zhang, Y. Zhao, D. Wang, J. Wang, Z. Zhang, X. Wang, Z. Chen, *Nano Energy* **2020**, *72*, 104685.

[61] R. Meng, Q. Du, N. Zhong, X. Zhou, S. Liu, S. Yin, X. Liang, *Adv. Energy Mater.* **2021**, *11*, 2102819.

[62] S. Wang, F. Huang, Z. Zhang, W. Cai, Y. Jie, S. Wang, P. Yan, S. Jiao, R. Cao, *J. Energy Chem.* **2021**, *63*, 336.

[63] M. Du, P. Geng, C. Pei, X. Jiang, Y. Shan, W. Hu, L. Ni, H. Pang, *Angew. Chem. Int. Ed.* **2022**, *61*, e202209350.

[64] X. Jiao, T. Deng, X. Men, Y. Zuo, J. Wang, *Ceram. Int.* **2022**, *48*, 16754.

[65] X. Wang, C. Zhao, B. Liu, S. Zhao, Y. Zhang, L. Qian, Z. Chen, J. Wang, X. Wang, Z. Chen, *Adv. Energy Mater.* **2022**, *12*, 2201960.

[66] D. Yang, Z. Liang, P. Tang, C. Zhang, M. Tang, Q. Li, J. J. Biendicho, J. Li, M. Heggen, R. E. Dunin-Borkowski, M. Xu, J. Llorca, J. Arbiol, J. R. Morante, S. L. Chou, A. Cabot, *Adv. Mater.* **2022**, *34*, 2108835.

[67] S. He, J. Yang, S. Liu, X. Wang, J. Qiu, *Adv. Funct. Mater.* **2023**, *34*, 2314133.

[68] Y. Xiao, S. Guo, Y. Xiang, D. Li, C. Zheng, Y. Ouyang, A. Cherevan, L. Gan, D. Eder, Q. Zhang, S. Huang, *ACS Energy Lett.* **2023**, *8*, 5107.

[69] Z. Zhu, Y. Zeng, Z. Pei, D. Luan, X. Wang, X. W. Lou, *Angew. Chem. Int. Ed.* **2023**, *62*, 202305828.

[70] S. Gu, S. Xu, X. Song, H. Li, Y. Wang, G. Zhou, N. Wang, H. Chang, *ACS Appl. Mater. Int.* **2022**, *14*, 50815.

[71] B. Y. Dang, D. Y. Gao, Y. H. Luo, Z. S. Zhang, J. D. Li, F. C. Wu, *J. Energy Storage* **2022**, *52*, 104981

[72] W. Li, X. Guo, P. Geng, M. Du, Q. Jing, X. Chen, G. Zhang, H. Li, Q. Xu, P. Braunstein, H. Pang, *Adv. Mater.* **2021**, *33*, 2105163.

[73] a) S. Hashemian, A. Sedrpoushan, F. H. Eshbala, *Catal. Lett.* **2017**, *147*, 196; b) W. Chen, C. Wang, S. Su, H. Wang, D. Cai, *Chem. Eng. J.* **2021**, *414*, 128784.

[74] Q. Wu, X. Zhao, T. Zhou, A. Jia, Y. Luo, J. Li, F. Wu, *J. Energy Storage* **2023**, *72*, 108596.

[75] S. Fu, H. Wang, Y. Zhong, S. Schaefer, M. Li, M. Wu, H. Wang, *Adv. Mater.* **2023**, *35*, e2302771.

[76] Y. Su, W. Wang, W. Wang, A. Wang, Y. Huang, Y. Guan, *J. Electrochem. Soc.* **2022**, *169*, 030528.

[77] X. Wang, Y. Wang, F. Wu, G. Jin, J. Li, Z. Zhang, *Appl. Surf. Sci.* **2022**, *596*, 153628.

[78] R. Razaq, M. M. U. Din, D. R. Småbråten, V. Eyupoglu, S. Janakiram, T. O. Sunde, N. Allahgoli, D. Rettenwander, L. Deng, *Adv. Energy Mater.* **2023**, *14*, 2302897.

[79] Y. Ni, L. Lin, Y. Shang, L. Luo, L. Wang, Y. Lu, Y. Li, Z. Yan, K. Zhang, F. Cheng, J. Chen, *Angew. Chem. Int. Ed.* **2021**, *60*, 16937.

[80] a) D. Su, M. Cortie, H. Fan, G. Wang, *Adv. Mater.* **2017**, *29*, 1700587; b) Y. Guo, P. Wu, H. Zhong, J. Huang, G. Ma, Z. Xu, Y. Wu, A. Zeb, X. Lin, *J. Colloid Interface Sci.* **2022**, *625*, 425

[81] G. Shen, Z. Liu, P. Liu, J. Duan, H. A. Younus, H. Deng, X. Wang, S. Zhang, *J. Mater. Chem. A* **2020**, *8*, 1154.

[82] M. Rana, H. A. Al-Fayaad, B. Luo, T. Lin, L. Ran, J. K. Clegg, I. Gentle, R. Knibbe, *Nano Energy* **2020**, *75*, 105009.

[83] X. Li, X. Zhang, Y. Xu, Y. Wang, Y. Huang, M. Ma, *Chem. Eur. J.* **2023**, *29*, e202300407.

[84] a) K. Zou, X. Chen, W. Jing, X. Dai, P. Wang, Y. Liu, R. Qiao, M. Shi, Y. Chen, J. Sun, Y. Liu, *Energy Storage Mater.* **2022**, *48*, 133; b) Y. Guo, Z. Jin, J. Lu, Z. Wang, Z. Song, A. Wang, W. Wang, Y. Huang, *Energy Environ. Mater.* **2023**, *7*, e12479; c) X. Zhu, W. Jiang, S. Zhao, R. Huang, M. Ling, C. Liang, L. Wang, *Nano Energy* **2022**, *96*, 107093.

[85] a) Z. Han, S. Zhao, J. Xiao, X. Zhong, J. Sheng, W. Lv, Q. Zhang, G. Zhou, H. M. Cheng, *Adv. Mater.* **2021**, *33*, 2105947; b) K. Liu, X. Wang, S. Gu, H. Yuan, F. Jiang, Y. Li, W. Tan, Q. Long, J. Chen, Z. Xu, Z. Lu, *Small* **2022**, *18*, 2204707; c) G. Liu, W. Wang, P. Zeng, C. Yuan, L. Wang, H. Li, H. Zhang, X. Sun, K. Dai, J. Mao, X. Li, L. Zhang, *Nano Lett.* **2022**, *22*, 6366; d) R. Xiao, T. Yu, S. Yang, K. Chen, Z. Li, Z. Liu, T. Hu, G. Hu, J. Li, H.-M. Cheng, Z. Sun, F. Li, *Energy Storage Mater.* **2022**, *51*, 890; e) J. Wang, L. Jia, S. Duan, H. Liu, Q. Xiao, T. Li, H. Fan, K. Feng, J. Yang, Q. Wang, M. Liu, J. Zhong, W. Duan, H. Lin, Y. Zhang, *Energy Storage Mater.* **2020**, *28*, 375; f) S. Hu, M. Yi, X. Huang, D. Wu, B. Lu, T. Wang, N. Li, Z. Zhu, X. Liu, J. Zhang, *J. Mater. Chem. A* **2021**, *9*, 2792.

[86] X. Hu, T. Huang, S. Wang, S. Lin, Z. Feng, L.-H. Chung, J. He, *Electrochim. Acta* **2021**, *398*, 139317.

[87] X. Li, Y. Xiao, Q. Zeng, L. Xu, S. Guo, C. Zheng, Q. Zhang, S. Huang, *Nano Energy* **2023**, *116*, 108813.

[88] a) S. Qiu, X. Liang, S. Niu, Q. Chen, G. Wang, M. Chen, *Nano Res.* **2022**, *15*, 7925; b) D. Yang, M. Li, X. Zheng, X. Han, C. Zhang, J.

Jacas Biendicho, J. Llorca, J. Wang, H. Hao, J. Li, G. Henkelman, J. Arbiol, J. R. Morante, D. Mitlin, S. Chou, A. Cabot, *ACS Nano* **2022**, *16*, 11102; c) C. Huang, J. Yu, C. Li, Z. Cui, C. Zhang, C. Zhang, B. Nan, J. Li, J. Arbiol, A. Cabot, *Adv. Funct. Mater.* **2023**, *33*, 2305624.
[89] H. Wu, Y. Yang, W. Jia, R. Xiao, H. Wang, *J. Alloys Compd.* **2021**, *874*, 159917.
[90] X. Zhang, G. Li, Y. Zhang, D. Luo, A. Yu, X. Wang, Z. Chen, *Nano Energy* **2021**, *86*, 106094.
[91] X. Wang, X. Zhang, Y. Zhao, D. Luo, L. Shui, Y. Li, G. Ma, Y. Zhu, Y. Zhang, G. Zhou, A. Yu, Z. Chen, *Angew. Chem. Int. Ed.* **2023**, *62*, e202306901.
[92] a) J. Zhou, X. Yu, X. Fan, X. Wang, H. Li, Y. Zhang, W. Li, J. Zheng, B. Wang, X. Li, *J. Mater. Chem. A* **2015**, *3*, 8272; b) Y. Mao, G. Li, Y. Guo, Z. Li, C. Liang, X. Peng, Z. Lin, *Nat. Commun.* **2017**, *8*, 14628.
[93] D.-S. Huang, X.-F. Qiu, J.-R. Huang, M. Mao, L. Liu, Y. Han, Z.-H. Zhao, P.-Q. Liao, X.-M. Chen, *Nat. Synth.* **2024**. DOI: 10.1038/s44160-024-00603-8.

Manuscript received: July 31, 2024
Revised manuscript received: September 14, 2024
Accepted manuscript online: September 24, 2024
Version of record online: October 30, 2024